New variables for the Lemaître-Tolman-Bondi dust solutions.

Roberto A. Sussman[†] and Luis García Trujillo[‡]
[†] *Instituto de Ciencias Nucleares, Apartado Postal 70543, UNAM, México DF, 04510, México.*
[‡] *Instituto de Física, Universidad de Guanajuato, Leon, Guanajuato, México.*

We re-examine the Lemâitre-Tolman-Bondi (LTB) solutions with a dust source admitting symmetry centers. We consider as free parameters of the solutions the initial value functions: Y_i, ρ_i, ${}^{(3)}\mathcal{R}_i$, obtained by restricting the curvature radius, $Y \equiv \sqrt{g_{\theta\theta}}$, the rest mass density, ρ, and the 3-dimensional Ricci scalar of the rest frames, ${}^{(3)}\mathcal{R}$, to an arbitrary regular Cauchy hypersurface, $\mathcal{T}_i$, marked by constant cosmic time ($t = t_i$). Using Y_i to fix the radial coordinate and the topology (homeomorphic class) of $\mathcal{T}_i$, and scaling the time evolution in terms of an adimensional scale factor $y = Y/Y_i$, we show that the dynamics, regularity conditions and geometric features of the models are determined by ρ_i, ${}^{(3)}\mathcal{R}_i$ and by suitably constructed volume averages and contrast functions expressible in terms of invariant scalars defined in $\mathcal{T}_i$. These quantities lead to a straightforward characterization of initial conditions in terms of the nature of the inhomogeneity of $\mathcal{T}_i$, as density and/or curvature overdensities ("lumps") and underdensities ("voids") around a symmetry center. In general, only models with initial density and curvature lumps evolve without shell crossing singularities, though special classes of initial conditions, associated with a simmultaneous big bang, allow for a regular evolution for initial density and curvature voids. Specific restrictions are found so that a regular evolution for $t > t_i$ is possible for initial voids. A step-by-step guideline is provided for using the new variables in the construction of LTB models and for plotting all relevant quantities.

I. INTRODUCTION

Lemaître-Tolman-Bondi metrics with a dust source and a comoving and geodesic 4-velocity constitute a well known class of exact solutions of Einstein's field equations [21] [22]. Under the prevailing conditions of a present day, standard, matter domminated universe, a dust momentum-energy tensor is a good approximation to non-relativistic matter sources. This fact, together with their mathematical simplicity, makes LTB solutions adequate models of inhomogeneous configurations of non-relativistic and collisionless matter (either barions or CDM). The relevance of such models is evident as they complement the usual perturbative approach by allowing one to study a case of exact non-linear evolution of inhomogeneities [10] [27] [22] [19]. Also, recent literature [8] [25] illustrates how a nearly isotropic CMB might not rule out an inhomogeneous universe compatible with current CBR observations.

The process of integration of the field equations for an LTB metric with a dust source in a comoving frame is very straightforward. This process, reviewed in section II, leads to a Friedmann-like dynamical equation for the curvatue radius $Y = \sqrt{g_{\theta\theta}}$, containing two arbitrary functions of the radial coordinate: $M(r)$ and $E(r)$. The integration of the dynamical equation yields a third arbitrary function, $t_{_{bb}}(r)$. The first two of these functions (M and E) are usualy identified as the relativistic analogues of the newtonian mass and the local energy associated with the comoving dust shells, the third function ($t_{_{bb}}$) can be interpreted as the "bang time", marking the proper time for the initial (or final) singularity for each comoving oberver. The functions M, E, $t_{_{bb}}$ are then the free parameters of the solutions, though any one of them can always be used to fix the radial coordinate, thus there are realy only two free functions. Regularity conditions, related to well behaved symmetry centers, abscence of shell crossing singularities and surface layers, can be given as restrictions on these functions and their radial gradients. These functions are usualy selected by means of convenient ansatzes based on the interpretations described above and/or the compatibility with regularity conditions or observational criteria. Once the free parameters have been selected we have a completely determined LTB model.

Since the standard free functions lead to a consistent description of LTB models, these free functions are used in most literature dealing with these solutions (see [22] for a comprehensive and autoritative review of this literature). There are papers considering specific modifications of the standard free functions in order to formulate initial conditions for studying the censorship of singularities [20], or aiming at an "intial value" formulation of LTB models [9]. We believe that new variables, defined along an arbitrary and regular "initial" hypersurface $t = t_i$, lead to a more intuitive understanding of LTB solutions. Therefore, we propose in this paper using a new set of basic free functions along the following steps

- Consider the rest mass density, ρ, the 3-dimensional Ricci scalar, ${}^{(3)}\mathcal{R}$, and the curvature radius, Y, all of them evaluated along an arbitrary Cauchy hypersurface, $\mathcal{T}_i$, marked by constant cosmic time $t = t_i$. This leads to: $\rho_i(r)$, ${}^{(3)}\mathcal{R}_i(r)$ and $Y_i(r)$, where the subindex $_i$ indicates evaluation along at $t = t_i$ (we shall use this convention henceforth).

- Rescale Y with Y_i, leading to an adimensional scale factor $y = Y/Y_i$, so that we can distinguish between the regular vanishing of Y (at a symmetry center, now given as $Y_i = 0$) and a central singularity (now characterized as $y = 0$). Likewise, we can distinguish between the two different situations when $Y' = 0$: regular vanishing or surface layers if $Y_i' = 0$ for a single value of r (thus restricting gradients of ρ_i and ${}^{(3)}\mathcal{R}_i$) and shell crossings when $\Gamma = (Y'/Y)/(Y_i'/Y_i) = 0$.
- Among the three free functions, $\rho_i(r)$, ${}^{(3)}\mathcal{R}_i(r)$ and $Y_i(r)$, we fix the radial coordinate (as well as the topology of $\mathcal{T}_i$) by a convenient selection of Y_i, using the remaining two functions as initial value functions.
- From the latter functions we can construct suitable volume averages and contrast functions, all of which expressible in terms of invariant scalars defined in $\mathcal{T}_i$. These auxiliary functions provide a clear cut and precise characterization of the nature of the initial inhomogeneity around a symmetry center, as overdensities ("lumps") or underdensities ("voids") of ρ_i and ${}^{(3)}\mathcal{R}_i$.

The old functions M, E, $t_{_{bb}}$ and their gradients can always be recovered and expressed in terms of the above mentioned volume averages and contrast functions. Hence, all known regularity conditions given in the old variables can easily be recast in terms of the new ones. In particular, the known conditions for avoiding shell crossing singularities [15] (see also [16] and [17]) have a more appealing and elegant form with the new variables, since with the old variables the signs of the gradients M', E', $t_{_{bb}}'$ do not distinguish manifestly between lumps or voids. In terms of the new variables, it is evident that, in general, shell crossings are avoided only for lumps of ρ_i and ${}^{(3)}\mathcal{R}_i$. However, some particular cases of initial conditions, such as a "simmultaneous bang time" ($t_{_{bb}}' = 0$), do allow for some initial conditions given as voids to evolve without shell crossings. If we consider an evolution in the time range $t > t_i$, then (under specific restrictions) initial voids can also evolve without shell crossings. All these features could also emerge with the old free functions, but the new variables provide a more straightforward and intuitive characterization of the effect of initial conditions in the regular evolution of LTB models.

The new approach to LTB dust solutions presented in this paper accounts, not only for an initial value treatment on a regular Cauchy hypersurface $\mathcal{T}_i$, but to a new formalism based on rescaling the evolution of the models to variables defined in this hypersurface. Some aspects of this formalism (average and contrast functions) have been developed elsewhere (see [26] and [28] for applications of LTB metrics with viscous fluid sources). Variables similar to the ones introduced here have been defined in [2], [20], [9], [23] and [10] (the latter in connection with Szekeres dust solutions, see equations 2.4.8 to 2.4.14 of [22]). Mena and Tavakol [11] have claimed that some of these variables are not covariant, thus suggesting covariant expressions for density contrasts (see also [24]). Although we show that the new variables can be expressed in terms of invariant scalars, and so are coordinate independent and can be computed for any coordinate system, we do not claim that the density and curvature averages and contrast functions introduced here have a clear "covariant interpretation", or that they are unique. However, what we can certainly claim is that these new variables emerge naturaly from the field equations, provide an adequate initial value treatment and yield a clear and concise description of regularity conditions.

The paper is organized as follows: section II reviews the basic expressions (metric, evolution equation and its solutions) characteristic of LTB models in the usual variables. The new variables are introduced in section III, leading to new forms for the metric, the rest mass density and the solutions of the evolution equation. Volume averages and contrast functions along $\mathcal{T}_i$ are defined in section IV. Section V examines in detail generic properties of the new variables: regularity, symmetry centers and geometric features of the hypersurface $\mathcal{T}_i$ (subsection V A), characterization of singularities (subsection V B), choice of radial coordinate and homeomorphic class (topology) of $\mathcal{T}_i$ (subsection V C), expressing the new variables in terms of invariant scalars (subsection V D), FLRW and Schwarzschild (subsection limits V E). In section VI we look at the characterization of the inhomogneity of $\mathcal{T}_i$ in terms density and 3-curvature "lumps" and "voids" and its relation with the contrast and average functions. In section VII we use the new variables in order to look at the conditions to avoid shell crossings, big bang times, regularity of the selected hypersurface $\mathcal{T}_i$ and simmultaneous big bang times. A summary of the no-shell-crossing conditions is given in Table 1. Section VIII provides simple functional ansatzes for the new variables and their auxiliary quantities (volume averages, contrast functions, as well as the old variables and the big bang times). A simple step-by-step guideline is provided for the construction of LTB models and for plotting all relevant quantities derived from these ansatzes. The characterization of intial conditions as "lumps" and "voids", as well as the fulfilment of the no-shell-crossing conditions is illustrated and tested graphicaly in 12 figures that complement the information provided in the text. Finaly, the Appendix provides a useful summary (in terms of the usual variables) of the generic geometric features of the solutions (regularity conditions, singularities, symmetry centers, surface layers).

Some important topics have been left out in this paper: time evolution of lumps and voids by generalizing volume averages and contrast functions to arbitrary times ($t \neq t_i$), models without centers, models with a mixed dynamics (elliptic and hyperbolic, etc), matchings of various LTB models, etc. The examination of these topics with the formalism presented here is currently in progress [29].

II. LTB SOLUTIONS, THE USUAL APPROACH.

Lemaitre-Tolman-Bondi (LTB) solutions are characterized by the line element

$$ds^2 \;=\; -c^2dt^2 \;+\; \frac{Y'^2}{1\,+\,E}\,dr^2 \;+\; Y^2\left[d\theta^2+\sin^2(\theta)d\phi^2\right] \tag{1}$$

where $Y=Y(t,r),\ E=E(r)$ and a prime denotes derivative with respect to r. The usual dust source associated with (1) is

$$T^{ab}=\rho\ u^a u^b, \tag{2}$$

where the 4-velocity is comoving $u^a=c\delta^a_t$. and $\dot{Y}=u^aY_{,a}=Y_{,ct}$. Einstein's field equations for (1) and (2) reduce to

$$\dot{Y}^2 \;=\; \frac{2\,M}{Y} \;+\; E, \tag{3}$$

$$\frac{4\pi G}{c^4}\,\rho \;=\; \frac{M'}{Y^2\,Y'}, \tag{4}$$

where

$$M \;\equiv\; \frac{4\pi G}{c^4}\,m(r), \tag{5}$$

and $m(r)$ is an arbitrary function (with units of energy) that emerges as an "integration constant". The form of the integrals (ie antiderivatives) of (3) depends on the sign of the function $E(r)$. Since (3) is the dynamical equation for LTB solutions, the usual convention classifies their possible dynamical evolution according to the three possible signs of E, as "parabolic" ($E=0$), "elliptic" ($E<0$) and "hyperbolic" ($E>0$). Two possible situations arise: either E has a specific (positive, negative or zero) sign for the full domain of regularity of r, or only for an open subset, $r_1<r<r_2$, possibly changing sign for other subsets of this domain. Whenever is necessary we will distinguish these two situations by using the terms "parabolic, elliptic or hyperbolic solutions" (full domain) and "parabolic, elliptic or hyperbolic regions" (subset). A convenient terminology that includes genericaly both situations is that of "parabolic, elliptic or hyperbolic dynamics".

Only for parabolic dynamics we can obtain a closed integral of (3) expressible in the form $Y=Y(t,r)$. For elliptic and hyperbolic dynamics we have either an implicit canonical solution of the form $c\,t-c\,t_{_{bb}}(r)=F(Y,r)$, were F is the integral quadrature of (3) and $t_{_{bb}}$ is an arbitrary function (ie an "integration constant"), or a parametric solution of the form $[Y(\eta,r),\ c\,t(\eta,r)-c\,t_{_{bb}}(r)]$. The function $t_{_{bb}}$ marks the proper time value corresponding to $Y=0$ for each comoving observer, hence it is customarily refered to as the "bang time". The solutions of (3) are

- Parabolic solution, $E=0,\ Y>0$:

$$Y^{3/2} \;=\; \pm\frac{3}{2}\sqrt{2\,M}\ c\ [\ t-t_{_{bb}}(r)\ ], \qquad\qquad t>t_{_{bb}}(+),\quad t<t_{_{bb}}(-) \tag{6}$$

- Elliptic solution, $E<0$, $0<Y<2M/|E|$:

$$c\,t(Y,r) \;=\; c\,t_{_{bb}}-\frac{\sqrt{Y(2M-|E|Y)}}{|E|}+\frac{M}{|E|^{3/2}}\arccos\left(1-\frac{|E|Y}{M}\right),$$
$$\dot{Y}>0, \qquad c\,t_{_{bb}}<c\,t<\frac{\pi\,M}{|E|^{3/2}},$$

$$c\,t(Y,r) \;=\; c\,t_{_{bb}}+\frac{\sqrt{Y(2M-|E|Y)}}{|E|}+\frac{M}{|E|^{3/2}}\left[2\pi-\arccos\left(1-\frac{|E|Y}{M}\right)\right],$$
$$\dot{Y}<0, \quad \frac{\pi\,M}{|E|^{3/2}}<c\,t<c\,t_{_{bb}}+\frac{2\pi\,M}{|E|^{3/2}}, \tag{7}$$

$$Y(\eta,r) \;=\; \frac{M}{|E|}\;[\,1\;-\;\cos\,\eta\,]\,, \tag{8}$$

$$c\,t(\eta,r) \;=\; c\,t_{_{bb}}\;+\;\frac{M}{|E|^{3/2}}\;[\,\eta\;-\;\sin\,\eta\,]\,, \tag{9}$$

- Hyperbolic solution, $E>0$:

$$\pm\;c\,(t-t_{_{bb}}) \;=\; \frac{\sqrt{Y\,(\,2M+E\,Y\,)}}{E}\;-\;\frac{M}{E^{3/2}}\,\mathrm{arccosh}\left(1+\frac{E\,Y}{M}\right), \tag{10}$$

$$Y(\eta,r) \;=\; \frac{M}{E}\;[\,\cosh\,\eta\;-\;1\,]\,, \tag{11}$$

$$c\,t(\eta,r) \;=\; c\,t_{_{bb}}\;\pm\;\frac{M}{E^{3/2}}\;[\,\sinh\,\eta\;-\;\eta\,]\,, \tag{12}$$

where the signs $\pm$ in the parabolic and hyperbolic cases distinguish between "expanding" or "collapsing" dust layers, that is Y increasing $(+)$ or decreasing $(-)$ as t increases, so that for any given layer $r=$ const., we have $t>t_{_{bb}}$ (expansion) and $t<t_{_{bb}}$ (collapse). Notice that the sign $\pm$ is not necessary in the elliptic case, since dust layers bounce (ie $\dot{Y}=0$) as $Y=2M/|E|$ and so both expansion and collapse are described by the same equations (8) and (9) and by each branch in the canonical solution (7).

As we mentioned before, $t_{_{bb}}(r)$ marks the proper time associated with $Y=0$ for each comoving layer (*ie* the "bang time"). The conventional interpretation for the other two free functions M and E is based on the analogue between the dynamical equation (3) and an energy equation in newtonian hydrodynamics (see [1]), in which M and E are usualy understood, respectively, as the "efective gravitational mass" and the "local energy per unit mass" associated with a given comoving layer. An alternative interpretation for E has been suggested as the local "embedding" angle of hypersurfaces of constant t ([12], [13], [11]). The specification or prescription of M and E is often made in the literature by selecting "convenient" mathematical ansatzes that are somehow intuitively based on these interpretations, loosely based on newtonian anlogues. However, configurations without centers [13] have no newtonian analogue and so the interpretation of M and E in this case is still an open question. Also, there is no newtonian equivalent for $t_{_{bb}}$ and no simple and intuitive way in which this function should be prescribed, though the gradient of this function has been shown to relate to growing/decreasing modes of dust perturbations in a FLRW background [10] [27] [14] [22], and thus the functional form of $t_{_{bb}}$ can be suggested from this feature.

III. NEW VARIABLES

A useful formulation of LTB solutions follows by redefining the free parameters M, E, $t_{_{bb}}$ in terms of an alternative set of new variables defined at a given arbitrary and fuly regular Cauchy hypersurface, $\mathcal{T}_i$, marked by $t=t_i$ (all such hypersurfaces are Cauchy hypersurfaces in LTB solutions [7]). In order to relate the free function E to the scalar 3-curvature of $\mathcal{T}_i$, we remark from (A3) that the Ricci scalar of these hypersurfaces is given by

$$^{(3)}\mathcal{R} \;=\; -\frac{2\,(E\,Y)'}{Y^2Y'}, \tag{13}$$

a relation expressible in terms of invariant scalars (see (A3) in the Appendix). We introduce

$$K \;\equiv\; -E, \tag{14}$$

so that the sign of $^{(3)}\mathcal{R}$ in (13) coincides with the sign of K. From here onwards we shall systematicaly replace E by $-K$, so that the type of dynamical evolution will now be denoted by the sign of K as: parabolic ($K=0$), hyperbolic ($K<0$) and elliptic ($K>0$). Bearing in mind (4), (13) and (14), we consider the following functions:

$$Y_i(r) \;\equiv\; Y(t_i,r), \tag{15}$$

$$\frac{4\pi G}{c^4}\,\rho_i(r) \;\equiv\; \frac{4\pi G}{c^4}\,\rho(t_i,r) \;=\; \frac{M'}{Y_i^2\,Y_i'}, \tag{16}$$

$$^{(3)}\mathcal{R}_i(r) \;\equiv\; {}^{(3)}\mathcal{R}(t_i,r) \;=\; \frac{2\,(K\,Y_i)'}{Y_i^2\,Y_i'}, \tag{17}$$

as initial value functions defined in $\mathcal{T}_i$. The subindex $_i$ will indicate henceforth evaluation along $t = t_i$. For the moment we will assume this hypersurface to be fuly regular, we discuss the corresponding regularity conditions in sections V A and VII.

In order to recast (3) and its solutions in terms of the new variables it is convenient to scale Y with respect to Y_i. By defining the adimensional scale variable

$$y \;\equiv\; \frac{Y}{Y_i}, \tag{18}$$

and using (14), (15), (16) and (17), equations (1), (3) and (4) become

$$ds^2 \;=\; -c^2\,dt^2 \;+\; y^2\left[\;\frac{\Gamma^2\,(Y_i')^2}{1-\kappa\,Y_i^2}\,dr^2 \;+\; Y_i^2\left(d\,\theta^2 \;+\; \sin^2\theta\,d\phi^2\right)\right], \tag{19}$$

$$\dot{y}^2 \;=\; \frac{2\,\mu}{y} \;-\; \kappa. \tag{20}$$

$$\rho \;=\; \rho_i\,\frac{Y_i^2\,Y_i'}{Y^2\,Y'} \;=\; \frac{\rho_i}{y^3\,\Gamma}, \tag{21}$$

where

$$\Gamma \;\equiv\; \frac{Y'/Y}{Y_i'/Y_i} \;=\; 1 \;+\; \frac{y'/y}{Y_i'/Y_i}, \tag{22}$$

$$\mu \;\equiv\; \frac{M}{Y_i^3}, \tag{23}$$

$$\kappa \;\equiv\; \frac{K}{Y_i^2}, \tag{24}$$

The solutions for the evolution equation (20) are those of (3), that is, equations (6) to (12) expressed in terms of the new variables y, μ, κ by means of (18), (23), (24) and by eliminating $t_{_{bb}}$ by setting $t = t_i$ and $Y = Y_i$ into equations (6) to (12). The solutions are

- Parabolic solution

$$y(t,r) \;=\; \left[\;1 \;\pm\; \frac{3}{2}\,\sqrt{2\,\mu}\;c(\;t \;-\; t_i\;)\;\right]^{2/3}, \tag{25}$$

- Elliptic solution

$$c\,t(y,r) \;=\; c\,t_i + \;\frac{[\;2\mu-\kappa\;]^{1/2} - [\;y\,(2\mu-\kappa\,y)\;]^{1/2}}{\kappa} \;+\; \frac{\mu}{\kappa^{3/2}}\left[\;\arccos\left(1-\frac{\kappa\,y}{\mu}\right) \;-\; \arccos\left(1-\frac{\kappa}{\mu}\right)\;\right],$$

$$\dot{y} > 0, \quad c\,t_{_{bb}} < c\,t_i < \frac{\pi\,\mu}{\kappa^{3/2}} \tag{26}$$

$$t(y,r) \;=\; c\,t_i + \;\frac{[\;2\mu-\kappa\;]^{1/2} + [\;y\,(2\mu-\kappa\,y)\;]^{1/2}}{\kappa} \;-\; \frac{\mu}{\kappa^{3/2}}\left[\;\arccos\left(1-\frac{\kappa\,y}{\mu}\right) \;+\; \arccos\left(1-\frac{\kappa}{\mu}\right) - 2\pi\;\right],$$

$$\dot{y} < 0, \quad \frac{\pi\,\mu}{\kappa^{3/2}} < c\,t < c\,t_{_{bb}} + \frac{2\pi\,\mu}{\kappa^{3/2}}, \tag{27}$$

$$y(\eta, r) \;=\; \frac{\mu}{\kappa}\,[\;1\;-\cos\,\eta\;]\,, \tag{28}$$

$$c\,t(\eta, r) \;=\; c\,t_i \;+\; \frac{\mu}{\kappa^{3/2}}\,[\;(\eta\;-\sin\,\eta)\;-\;(\eta_i\;-\;\sin\,\eta_i)\;]\,, \tag{29}$$

$$\eta \;=\; \arccos\left(1-\frac{\kappa\,y}{\mu}\right), \qquad \eta_i \;=\; \arccos\left(1-\frac{\kappa}{\mu}\right), \tag{30}$$

- Hyperbolic solution

$$c\,t(y, r) \;=\; c\,t_i \;\pm\; \frac{[\;y\,(2\mu+|\kappa|\,y)\;]^{1/2}-[\;2\mu+|\kappa|\;]^{1/2}}{|\kappa|} \;\pm\; \frac{\mu}{|\kappa|^{3/2}}\left[\;\mathrm{arccosh}\left(1+\frac{|\kappa|\,y}{\mu}\right)\;-\;\mathrm{arccosh}\left(1+\frac{|\kappa|}{\mu}\right)\;\right], \tag{31}$$

$$y(\eta, r) \;=\; \frac{\mu}{|\kappa|}\,[\;\cosh\,\eta\;-1\;]\,, \tag{32}$$

$$c\,t(\eta, r) \;=\; c\,t_i \;\pm\; \frac{\mu}{|\kappa|^{3/2}}\,[\;\;(\sinh\,\eta\;-\;\eta)\;-\;(\sinh\,\eta_i\;-\eta_i)\;]\,, \tag{33}$$

$$\eta \;=\; \mathrm{arccosh}\left(1+\frac{|\kappa|\,y}{\mu}\right), \qquad \eta_i \;=\; \mathrm{arccosh}\left(1+\frac{|\kappa|}{\mu}\right), \tag{34}$$

where, as before, the signs $\pm$ distinguish between expanding layers ($-$ sign, $t_{_{bb}}$ in the past of t_i) and collapsing ones ($+$ sign, $t_{_{bb}}$ in the future of t_i). Explicit forms for $t_{_{bb}}$ in terms of μ, κ, η_i and t_i are given in section VII.

It is important to remark that $y(t_i, r) = y_i = 1$, by definition, and so $y = 1$ corresponds to $t = t_i$. This is clear for the parabolic (25) and hyperbolic solutions (31) and (33). However, it is important to notice that $c\,t_i < \pi\mu/\kappa^{3/2}$ in (26) and so the initial hypersurface must be defined in the expanding phase in the elliptic solution. In this solution the correspondence between $t = t_i$ and $y = 1$ only holds in the expanding phase of (26) but not in its collapsing phase. The explanation is simple: in general the expanding and collapsing phases of the elliptic solution are not time-symmetric, as in the homogeneous FLRW case, therefore $y = 1$ will also be reached in the collapsing phase but it will not (in general) correspond to a single hypersurface $t =$ constant. Figure 1 illustrates this feature.

IV. VOLUME AVERAGES AND CONTRAST FUNCTIONS ALONG THE INITIAL HYPERSURFACE.

The definitions (16) and (17) of the initial value functions ρ_i and ${}^{(3)}\mathcal{R}_i$ lead to the following integrals

$$M(r) \;=\; \frac{4\pi G}{c^4}\int_{r_c}^{r}\rho_i\,Y_i^2\,Y_i'\,dr \tag{35}$$

$$K(r) \;=\; \frac{1}{2\,Y_i}\int_{r_c}^{r}{}^{(3)}\mathcal{R}_i\,Y_i^2\,Y_i'\,dr \tag{36}$$

where the lower integration limits in these integrals have been fixed by the conditions $M(r_c) = K(r_c) = 0$, where $r_1 = r_c$ marks a *Symmetry Center*[1] (to be denoted henceforth as "SC" or as "center", see section V A and the

[1] See section V A for more details. See the Appendix for a formal defintition of a Symmetry Center

Appendix). For the remaining of this paper we shall assume, unless explicitly specified otherwise, that the spacetime manifold admits at least one SC and so the integrals (35) and (36) become functions that depend only on the upper integration limit r.

Since $4\pi \int Y_i^2 Y_i' dr$ is the volume associated with the orbits of SO(3) in the hypersurface $\mathcal{T}_i$ (though it is not a proper volume related to (A12)), equations (35) and (36) suggest then the introduction of the following volume averages

$$\langle \rho_i \rangle(r) \;=\; \frac{\int^r \rho_i\, Y_i^2\, Y_i'\, dr}{\int^r Y_i^2\, Y_i'\, dr} \;=\; \frac{3\, m(r)}{Y_i^3}, \tag{37}$$

$$\langle {}^{(3)}\mathcal{R}_i \rangle(r) \;=\; \frac{\int^r {}^{(3)}\mathcal{R}_i\, Y_i^2\, Y_i'\, dr}{\int^r Y_i^2\, Y_i'\, dr} \;=\; \frac{6\, K(r)}{Y_i^2}, \tag{38}$$

In terms of these volume averages the variables μ and κ in (23) and (24) become

$$\mu \;=\; \frac{4\pi G}{3c^4}\, \langle \rho_i \rangle, \tag{39}$$

$$\kappa \;=\; \frac{1}{6}\, \langle {}^{(3)}\mathcal{R}_i \rangle, \tag{40}$$

Setting ρ_i and ${}^{(3)}\mathcal{R}_i$ to constants in equations (37) and (38) yields $\rho_i = \langle \rho_i \rangle$ and ${}^{(3)}\mathcal{R}_i = \langle {}^{(3)}\mathcal{R}_i \rangle$, therefore the comparison between ρ_i, ${}^{(3)}\mathcal{R}_i$ and $\langle \rho_i \rangle$, $\langle {}^{(3)}\mathcal{R}_i \rangle$ must provide a "gauge" that measures the inhomogeneity of ρ_i and ${}^{(3)}\mathcal{R}_i$ in the closed interval $r \geq r_c$. This motivates defining the following "inhomogeneity gauges" or contrast functions

$$\Delta_i^{(m)} \;=\; \frac{\rho_i}{\langle \rho_i \rangle} \;-\; 1, \qquad \Rightarrow \qquad \rho_i \;=\; \langle \rho_i \rangle \left[\, 1 \;+\; \Delta_i^{(m)} \right], \tag{41}$$

$$\Delta_i^{(k)} \;=\; \frac{{}^{(3)}\mathcal{R}_i}{\langle {}^{(3)}\mathcal{R}_i \rangle} \;-\; 1, \qquad \Rightarrow \qquad {}^{(3)}\mathcal{R}_i \;=\; \langle {}^{(3)}\mathcal{R}_i \rangle \left[\, 1 \;+\; \Delta_i^{(k)} \right], \tag{42}$$

These functions can be expressed in terms of M, K, μ and κ and their radial gradients. For example:

- $\Delta_i^{(m)}$ and $\Delta_i^{(k)}$ in terms of μ, M, κ, K

$$1 \;+\; \Delta_i^{(m)} \;=\; \frac{4\pi G}{3c^4}\, \frac{\rho_i}{\mu} \;=\; \frac{4\pi G}{3c^4}\, \frac{\rho_i\, Y_i^3}{M},$$

$$1 \;+\; \Delta_i^{(k)} \;=\; \frac{{}^{(3)}\mathcal{R}_i}{6\,\kappa} \;=\; \frac{{}^{(3)}\mathcal{R}_i\, Y_i^2}{6\, K}, \tag{43}$$

- $\Delta_i^{(m)}$ and $\Delta_i^{(k)}$ in terms of μ', M', κ', K' and Y_i'

$$1 \;+\; \Delta_i^{(m)} \;=\; \frac{M'/M}{3Y_i'/Y_i}, \qquad \frac{\mu'/\mu}{3Y_i'/Y_i} \;=\; \Delta_i^{(m)}, \tag{44}$$

$$1 \;+\; \frac{3}{2}\Delta_i^{(k)} \;=\; \frac{K'/K}{2Y_i'/Y_i}, \qquad \frac{\kappa'/\kappa}{3Y_i'/Y_i} \;=\; \Delta_i^{(k)}, \tag{45}$$

Another useful relation is

$$\frac{M'}{M} \;-\frac{3}{2}\,\frac{K'}{K} \;=\; \frac{\mu'}{\mu} \;-\frac{3}{2}\,\frac{\kappa'}{\kappa} \;=\; \frac{Y_i'}{Y_i}\left(\Delta_i^{(m)} \;-\; \frac{3}{2}\,\Delta_i^{(k)}\right), \tag{46}$$

The interpretation of $\Delta_i^{(m)}$ and $\Delta_i^{(k)}$ as contrast functions will be discussed in section VI. Using (44), (45) and (46) we can eliminate all radial gradients like μ', κ' (or M', K') in terms of $\Delta_i^{(m)}$ and $\Delta_i^{(k)}$. Since these gradients appear in the evaluation of Γ from (22) and the solutions of (20) (see section VII), it is certainly useful to be able to relate an important quantity like Γ to initial conditions expressed in terms of quantities like $\Delta_i^{(m)}$ and $\Delta_i^{(k)}$, quantities that have a more intuitive and appealing interpretation than M' and K'.

V. GENERIC PROPERIES OF THE NEW VARIABLES

We discuss in this section the regularity properties and generic features of the new variables, as well as their relation with M, K defined by (37), (38). The averages and contrast functions, (41) and (42), are examined in section VI. Frequent reference will be made to expressions presented and summarized in the Appendix.

A. Initial hypersurfaces.

A hypersurface $\mathcal{T}_i$ is the 3-dimensional submanifold obtained by restricting an LTB spacetime to $t = t_i$. This submanifold can be invariantly characterized as the set of rest frames of comoving observers associated with proper time $t = t_i$ (see the Appendix). Its induced 3-dimensional metric is

$$ds_i^2 \;=\; \frac{Y_i'^2}{1-\kappa\, Y_i^2}\, dr^2 \;+\; Y_i^2\,\left[\, d\theta^2 \;+\; \sin^2\theta\, d\phi^2\right], \tag{47}$$

where $0 \leq \theta \leq \pi$ and $0 \leq \phi \leq 2\pi$ and r extends along its domain of regularity (see subsection V C and the parragraph below). For a regular $\mathcal{T}_i$, all invariant scalars like (A3), (A4) and (A5) resticted to $t = t_i$, or invariant scalars computed directly from (47), must be bounded. The metric (47) is also subjected to the regularity condition (A7) which now reads

$$1 \;-\; K \;=\; 1 \;-\; \kappa\, Y_i^2 \;\geq\; 0 \qquad \Rightarrow \qquad \frac{1}{6}\,{}^{(3)}\mathcal{R}_i\, Y_i^2 \;=\; \frac{{}^{(3)}\mathcal{R}_i}{\langle {}^{(3)}\mathcal{R}_i\rangle}\, K \;\leq\; 1 \;+\; \Delta_i^{(k)}, \tag{48}$$

where the equality must coincide with a zero of Y_i' (see below) and we have used (14), (24), (38), (40) and (42). The hypersurface $\mathcal{T}_i$ can be foliated by the orbits of SO(3) marked bt $r = $ const., thus the regular domain of r is then limited, either by a SC, or by those maximal values $r = r_{\max}$ defined by (A11) restricted to $t = t_i$

$$\ell_i(r_1, r) \;=\; \int_{r_1}^{r} \frac{Y_i'\, dr}{\sqrt{1-K}} \;=\; \int_{r_1}^{r} \frac{Y_i'\, dr}{\sqrt{1-\kappa\, Y_i^2}} \;=\; \int_{r_1}^{r} \frac{\left[1+\Delta_i^{(k)}\right]^{1/2} Y_i'\, dr}{\left[1+\Delta_i^{(k)}+\frac{1}{6}{}^{(3)}\mathcal{R}_i\, Y_i^2\right]^{1/2}} \;\to\; \infty \quad \text{as} \quad r \to r_{\max} \tag{49}$$

where $\mathcal{K}$ and κ have been eliminated in terms of ${}^{(3)}\mathcal{R}_i$ and $\Delta_i^{(k)}$ by means of (40) and (42). These maximal values could correspond to $r \to \infty$ or $r \to \pm\infty$, but this is not necessary, as it is always possible to define the radial coordinate so that maximal values $r_{\max}$ correspond to finite values of r (see section V C).

- Regularity and differentiability.

  From their definition in (16), (17) and (15), the functions ρ_i, ${}^{(3)}\mathcal{R}_i$, Y_i satisfy the same regularity and differentiability conditions as ρ, ${}^{(3)}\mathcal{R}$, Y in the radial direction (see the Appendix): $Y_i \geq 0$ must be continuous and $\rho_i \geq 0$, ${}^{(3)}\mathcal{R}_i$ can be piecewise continuous but with a countable number of finite jump discontinuities. The average functions, $\langle\rho_i\rangle$, $\langle {}^{(3)}\mathcal{R}_i\rangle$, constructed from intergration of ρ_i, ${}^{(3)}\mathcal{R}_i$, will be, in general continuous (like M and K). The contrast functions, $\Delta_i^{(m)}$ and $\Delta_i^{(k)}$, explicitly contain ρ_i and ${}^{(3)}\mathcal{R}_i$ (from (43)), hence they are, at least, piecewise continuous.

- Zeroes of Y_i and Y_i'.

  The zeroes of Y_i and Y_i' are also zeroes of Y and Y', though the converse is not (in general) true. Because of (15) all regular zeroes of Y and Y', associated with a comoving r (symmetry centers and turning values of Y') will be shared by Y_i, but a regular $\mathcal{T}_i$ must avoid the zeroes of Y and Y' that do not correspond to a comoving r (singular zeroes). Therefore, we have along $\mathcal{T}_i$

  - Symmetry Centers, SC..

    Let $r = r_c$ mark a SC (see the Appendix). The functions Y_i, ρ_i, ${}^{(3)}\mathcal{R}_i$, from their definitions in (15), (16) and (17), must satisfy

$$
\begin{array}{lll}
Y_i(r_c)=0, \quad Y_i'(r_c)=S_i\neq 0, & & Y_i\approx S_i(r-r_c) \\
\rho_i(r_c)>0 & \rho_i'(r_c)=0 & \rho_i\approx \rho_i(r_c)+\frac{1}{2}\rho_i''(r_c)(r-r_c)^2 \\
{}^{(3)}\mathcal{R}_i(r_c)\neq 0 & {}^{(3)}\mathcal{R}_i'(r_c)=0 & {}^{(3)}\mathcal{R}_i\approx {}^{(3)}\mathcal{R}_i(r_c)+\frac{1}{2}{}^{(3)}\mathcal{R}_i''(r_c)(r-r_c)^2 \\
{}^{(3)}\mathcal{R}_i(r_c)=0 & {}^{(3)}\mathcal{R}_i'(r_c)=0 & {}^{(3)}\mathcal{R}_i(r)=0, \quad \text{parabolic dynamics}
\end{array}
\tag{50}
$$

where $S_i = S(t_i) = Y'(t_i, r_c) > 0$ and the fourth subcase above denotes the case of parabolic dynamics in which the condition $K = \kappa = 0$ holds in an interval $r_c \leq r$, thus implying that ${}^{(3)}\mathcal{R}_i(r) = 0$ for all the interval. The central behavior of M, K in (35) and (36) is given by the leading terms

$$
\begin{aligned}
M &\approx \frac{4\pi G}{3c^4}\,\rho_i(r_c)\,S_i^3\,(r-r_c)^3, \\
K &\approx \frac{1}{6}\,{}^{(3)}\mathcal{R}_i(r_c)\,S_i^2\,(r-r_c)^2,
\end{aligned}
\tag{51}
$$

From (23), (24), (39), (40), (41) and (42), the value of μ, κ and the remaining initial value functions at $r = r_c$ are given by

$$
\begin{aligned}
\mu(r_c) &= \frac{4\,\pi\,G}{3c^4}\,\rho_i(r_c), \qquad \kappa(r_c) = \frac{1}{6}\,{}^{(3)}\mathcal{R}_i(r_c), \\
\langle\rho_i\rangle(r_c) &= \rho_i(r_c), \qquad \langle{}^{(3)}\mathcal{R}_i\rangle(r_c) = {}^{(3)}\mathcal{R}_i(r_c), \qquad \Rightarrow \qquad \Delta_i^{(m)}(r_c) = \Delta_i^{(k)}(r_c) = 0,
\end{aligned}
\tag{52}
$$

– Signs and turning values of Y_i'.
From (15) and comparing (4) with (16) and (13) with (17), it is evident that regularity of ρ and ρ_i requires the sign of Y_i' to be the same as the sign of Y'. Hence condition (A6) can be restated as

$$
\rho_i \geq 0 \qquad \Leftrightarrow \qquad \text{sign}(M') = \text{sign}(Y_i'),
\tag{53}
$$

so that regularity of ρ_i, ${}^{(3)}\mathcal{R}_i$ and of the metric (47) leads to the condition that all the following equations

$$
Y_i'(r^*) = 0, \qquad M'(r^*) = 0, \qquad 1 - K(r^*) = 0, \qquad (K\,Y_i)' = 0,
\tag{54}
$$

must have common zeroes (turning values), $r = r^*$, of the same order in $r - r^*$. Failure to comply with (54), not only reflects "bad" choices of ρ_i, ${}^{(3)}\mathcal{R}_i$, but leads to surface layers in $r = r^*$ associated with a discontinuous extrinsic curvature of the submanifold $r = r^*$ [30], [4], [16], [17], [18].

B. Comparison of y vs Y and Γ vs Y'.

Since the zeroes of $\{Y = 0, Y' = 0\}$ do not (in general) imply $\{Y_i = 0, Y_i' = 0\}$, but all comoving zeroes of $\{Y = 0, Y' = 0\}$ are also zeroes of $\{Y_i = 0, Y_i' = 0\}$, those zeroes of $\{Y = 0, Y' = 0\}$ that are not common to $\{Y_i = 0, Y_i' = 0\}$ must correspond to curvature singularities (central or shell crossing). This removes the ambigueity of identifying these singularities by the constraints $Y = 0$ and $Y' = 0$, placing this identification on y and Γ. From its definition in (18), it is evident that $y(t_i, r) = 1$, while its central behavior is given by

$$
y(t, r_c) = \frac{S(t)}{S_i}, \qquad y(t, r) \approx \frac{S(t)}{S_i}\,[\,1 + O(r - r_c) + O(t - t_i)]\,,
\tag{55}
$$

where $S(t) = Y'(t, r_c)$, so that (in general) y does not vanish at a SC. This means that $y = 0$ implies $Y = 0$, but the converse is false, since $Y = 0$ does not imply $y = 0$ (for example at $r = r_c$). Therefore, the coordinate locus for a central singularity (either big bang or big crunch) becomes

$$
y(t, r) = 0, \qquad \text{Central singularity.}
\tag{56}
$$

an unambiguous characterization, as opposed to $Y = 0$ which can be associated either to such a singularity or to a SC. In fact, as mentioned in the previous section and from the form of the metric (19), the function y plays the role of a local scale factor, in contrast to Y defined non-localy in terms of the proper surface of the orbits of SO(3) around

a SC that might not even be contained in the spacetime manifold. The difference between y and Y is illustrated in figures 2 displaying parametric 3d plots $Y(t,r)$ and $y(t,r)$ for various LTB models. These figures clearly show that $y(t_i)=1$ for all layers.

From (A8), the gradient Y'/Y is singular at a SC, however, from (21), (22) and (55), we have

$$\Gamma(t,r_c) \;=\; 1, \qquad \rho(t,r_c) \;=\; \rho_i(r_c)\,\frac{S_i^3}{S^3(t)}, \qquad \sigma(t,r_c) \;=\; 0, \qquad \Theta(t,r_c) \;=\; \frac{3\,\dot{S}(t)}{S(t)} \tag{57}$$

while the coordinate locus for shell crossing singularities can be given as

$$\Gamma \;=\; 0, \quad \rho_i \;>\; 0, \qquad \text{Shell crossing singularity.} \tag{58}$$

a characterization that avoids the ambigueity of $Y'=0$, since, as mentioned in the Appendix, Y' might vanish and change sign regularly for a single $r=r^*\neq r_c$ if (A9) holds, preventing surface layers. This situation is now taken care by conditions (54) acting on Y_i'.

C. The function Y_i: choice of topology and radial coordinate.

From the common geometric meaning of Y and Y_i (see Appendix), it is evident that the homeomorphic class ("open" or "closed" topology) of the regular hypersurfaces of constant t follows from the homeomorphic class of $\mathcal{T}_i$. The latter can be determined by applying (A12) to (47) for a given choice of $Y_i(r)$, along the domain of regularity of r limited between SC's (real roots of $Y_i(r)=0$) and/or a maximal value $r_{\max}$ defined by (49). Because we can always rescale r, it is always possible to select this coordinate so that Y_i takes the simplest form, hence the freedom to select Y_i can also be the freedom to find a convenient radial coordinate for a desired LTB configuration. As mentioned in the Appendix, the compatibility of any one of the possible choices of homeomorphic class with any one of the three choices of dynamical evolution (parabolic, hyperbolic or elliptic) is only restricted by the regularity conditions (48), (54) and (49). We ellaborate these issues below looking separately the case with one and two SC's.

- One symmetry center.

  Since we can always mark the SC by $r=0$, then $Y_i(0)=0$ and if Y_i is a monotonously increasing (one-to-one) function ($Y_i'>0$) for all r, we can then choose the radial coordinate so that $Y_i=S_i\,r$, where S_i is a characteristic constant length. This is equivalent to using Y_i/S_i as a new radial adimensional coordinate, but we can also set $Y_i=S_i\,f(r)$, for any monotonously increasing function with $f(r_c)=0$. The range of r is $0\leq r<r_{\max}$, so that proper distances ℓ_i increase as r grows and $\ell_i\to\infty$ as $r\to r_{\max}$. A useful coordinate choice is $f=\tan r$, so that maximal values associated with $Y_i\to\infty$ can be mapped to $r=\pi/2$. Fulfilment of conditions (48), (54) and (49) is trivial for parabolic and hyperbolic dynamics, but for elliptic dynamics we must have $K\to 1$ as $r\to r_{\max}$. The homeomorphic class is $\mathbf{R^3}$.

- Two symmetry centers.

  Let the centers be marked by $r=r_{c_1}$ and $r=r_{c_2}$. Then $Y_i(r_{c_1})=Y_i(r_{c_2})=0$, so that Y_i' vanishes for some r^* in the open interval $r_{c_1}<r^*<r_{c_2}$. In this case, it is not possible to rescale Y_i with r because Y_i is not a one-to-one function of r. However, depending on the model under consideration, it is always possible to select the radial coordinate so that $Y_i=S_i\,f(r)$, where $f(r)$ is a C^0 function satisfying $f(r_{c_1})=f(r_{c_2})=0$ and $f'(r^*)=0$, so that ${\rho_i}',{}^{(3)}\mathcal{R}_i'$, M', K', $1-K=1-\kappa Y_i^2$ all vanish at r^* and have zeroes of the same order on $r-r^*$. Since the hypersurface $t=t_i$ has a finite proper volume, ℓ_i evaluated from one SC to the other (the maximal range of r) must be finite. Although it is possible to set $K\leq 0$ (parabolic and hyperbolic evolution), only for elliptic evolution it is possible to fulfil condition (54) in order to avoid surface layers in $r=r^*$ (see [4], [16] and [18]). The hypersurface $\mathcal{T}_i$ is homeomorphic to a 3-sphere, $\mathbf{S^3}$.

D. Invariant expressions.

The volume averages and contrast functions introduced in section IV were constructed by averaging ρ_i and ${}^{(3)}\mathcal{R}_i$ with the volume $(4/3)\,\pi\,Y_i^3=4\,\pi\int Y_i^2\,Y_i'\,dr$, a quantity that can be related to the proper area, $4\pi\,Y_i^2$, of the group orbits of SO(3). However, it can be argued that these volume averages and contrast functions are coordinate dependent expressions. We can show that these quantities are equivalent to coordinate independent expressions given in terms of invariant scalars evaluated along $\mathcal{T}_i$. From (A4) and (A5) applied to $t=t_i$, together with (41), we obtain

$$\frac{8\pi G}{c^4}\,\langle\rho_i\rangle \;=\; \frac{8\pi G}{c^4}\,\rho_i \;+\; 6\,[\psi_2]_i \;=\; \mathcal{R}_i \;+\; 6\,[\psi_2]_i$$

$$1 \;+\; \Delta_i^{(m)} \;=\; \frac{4\pi G\,\rho_i}{4\pi G\,\rho_i \;+\; 3\,c^4\,[\psi_2]_i} \;=\; \frac{\mathcal{R}_i}{\mathcal{R}_i \;+\; 6\,[\psi_2]_i}, \tag{59}$$

where $\mathcal{R}_i$ and $[\psi_2]_i$ are the 4-dimensional Ricci scalar and the conformal invariant ψ_2 evaluated at $t = t_i$. The evolution equation (20) applied to $t = t_i$, together with (A2), (A3), (39), (40), (42) and (59) yields

$$\frac{c^2}{2}\,\langle {}^{(3)}\mathcal{R}_i\rangle \;=\; \frac{c^2}{2}\,{}^{(3)}\mathcal{R}_i \;-\; 6\,\sigma_i\left(\sigma_i + \frac{\Theta_i}{3}\right) \;=\; c^2\,\mathcal{R}_i \;+\; 6\,c^2\,[\psi_2]_i \;-\; 3\left(\sigma_i + \frac{\Theta_i}{3}\right)^2,$$

$$1 \;+\; \Delta_i^{(k)} \;=\; \frac{c^2\,\mathcal{R}_i \;+\; 3\,[\,\sigma_i^2 - (\frac{1}{3}\Theta_i)^2\,]}{c^2\,\mathcal{R}_i \;+\; 6\,c^2\,[\psi_2]_i \;-\; (\,\sigma_i \;+\; \frac{1}{3}\Theta_i\,)^2} \;=\; \frac{c^2\,{}^{(3)}\mathcal{R}_i}{c^2\,{}^{(3)}\mathcal{R}_i \;-\; 12\,\sigma_i\,(\sigma_i + \frac{1}{3}\Theta_i)}, \tag{60}$$

where σ_i and Θ_i are the kinematic invariants appearing in (A1) and (A2) (the expansion scalar and the degenerate eigenvalue of the shear tensor) evaluated along $\mathcal{T}_i$. The expressions (59) and (60) are not the definitive "covariant interpretations" for the average and contrast functions. They have been presented in order to emphasize that these quantities can be expressed in terms of invariant scalars and so can be computed in any coordinate system. An alternative volume averaging could have been attempted using the proper volume (A12), leading to quantities like

$$\frac{\int \rho_i\,(1-K)^{-1/2}\,Y_i^2\,Y_i'\,dr}{\int (1-K)^{-1/2}\,Y_i^2\,Y_i'\,dr}, \qquad \frac{\int {}^{(3)}\mathcal{R}_i\,(1-K)^{-1/2}\,Y_i^2\,Y_i'\,dr}{\int (1-K)^{-1/2}\,Y_i^2\,Y_i'\,dr}, \tag{61}$$

instead of the volume averages in (37) and (38). Notice that only for parabolic dynamics all these averages coincide. We have chosen to use (37) and (38) instead of (61) mostly because the former are mathematicaly simpler than the latter and because they follow naturaly from the field and evolution equations. For example, the functions $M, E = -K$ or μ, κ that appear in the solutions of (3) or (20) immediately relate to (37) and (38), but their relation with (61) is (except for parabolic dynamics) mathematicaly difficult, making it very hard to accomodate quantities like (61) to the dynamical study of the models. Since all the invariant scalars defined in $\mathcal{T}_i$ by (59) and (60) can be generalized for arbitrary times $t \neq t_i$, the volume averages and contrast functions can also be generalized in this manner. For example, the fact that $M = M(r)$ and $K = K(r)$, and so these functions are constants for every comoving oberver, follows (from (37) and (38)) from the conservation (along the 4-velocity flow) of quantities like $\langle\rho\rangle Y^3$ and $\langle {}^{(3)}\mathcal{R}\rangle Y^2$, were $\langle\rho\rangle$ and $\langle {}^{(3)}\mathcal{R}\rangle$ are the generalization to arbitrary times of $\langle\rho_i\rangle$ and $\langle {}^{(3)}\mathcal{R}_i\rangle$. This and other conservation laws are being examined elsewhere [29].

E. FLRW and Schwarzschild limits, matchings and hybrid models.

It is a well known fact that LTB solutions contain as particular cases FLRW cosmologies with dust source (homogeneous and isotropic limit) and the Schwarzschild-Kruskal spacetime (vacuum limit). We examine these limits below

- FLRW limit. If for all the domain of regularity of r we have $\rho_i = \rho_i^{(0)}$ and ${}^{(3)}\mathcal{R}_i = {}^{(3)}\mathcal{R}_i^{(0)}$, where $\rho_i^{(0)} \geq 0$ and ${}^{(3)}\mathcal{R}_i^{(0)}$ are constants, then equations (37), (38), (41) and (42) imply

$$\rho_i \;=\; \langle\rho_i\rangle \;=\; \rho_i^{(0)}, \qquad \Rightarrow \qquad \Delta_i^{(m)} \;=\; 0, \qquad M \;=\; \frac{4\pi G}{3c^4}\,\rho_i^{(0)}\,Y_i^3$$

$${}^{(3)}\mathcal{R}_i \;=\; \langle {}^{(3)}\mathcal{R}_i\rangle \;=\; {}^{(3)}\mathcal{R}_i^{(0)}, \qquad \Rightarrow \qquad \Delta_i^{(k)} \;=\; 0, \qquad K \;=\; \frac{1}{6}\,{}^{(3)}\mathcal{R}_i^{(0)}\,Y_i^2, \tag{62}$$

  Since μ and κ in (23) and (24) are now constants, y (determined by (20)) must be a function of t only, and so, from (18) and (22), we have $\Gamma = 1$ and $Y = (S(t)/S_i)\,Y_i$, identifying $y = S(t)/S_i$ with an adimensional FLRW scale factor. Rest mass density and scalar 3-curvature take the FLRW forms: $\rho = \rho_i^{(0)}\,(S_i/S)^3$ and ${}^{(3)}\mathcal{R} = {}^{(3)}\mathcal{R}_i^{(0)}\,(S_i/S)^2$, while the metric (19) becomes a FLRW metric if we identify $Y_i = S_i\,r$ so that $(1/6)\,{}^{(3)}\mathcal{R}_i^{(0)} S_i^2$ becomes an adimensional curvature index. Equations (62) reafirm the role of inhomogeneity gauges for $\Delta_i^{(m)}$ and $\Delta_i^{(k)}$, making also evident that initial conditions with homogeneous ρ_i and ${}^{(3)}\mathcal{R}_i$ leads only to FLRW evolution.

- Schwarzschild limit. For an intial density given by a normalized Dirac delta (a point mass)

$$\rho_i = \rho_i^{(0)}\,\delta(Y_i^3) = \rho_i^{(0)}\,S_i^3\,\delta(r^3) \tag{63}$$

we obtain: $m = \rho_i^{(0)}\,S_i^3/3$ from (35), so that we can identify the "Schwarzschild mass" with $2M$ given by (5). The metric (1), together with (3) with $M =$ const. describes the Schwarzschild-Kruskal spacetime in terms of the worldlines of geodesic test observers with 4-velocity u^a. The function ${}^{(3)}\mathcal{R}$ is the scalar 3-curvature of the hypersurfaces of simmultaneity of these congruences.

If only one of ρ_i or ${}^{(3)}\mathcal{R}_i$ is constant (but nonzero) in a domain of r containing a SC, then only $\Delta_i^{(m)}$ or $\Delta_i^{(k)}$ vanishes in this domain. For hyperbolic or elliptic dynamics, these are special cases of initial conditions but do not correspond to the FLRW limit (for parabolic dynamics ${}^{(3)}\mathcal{R}_i = 0$ and so the FLRW limit follows from $\rho_i = \rho_i^{(0)} > 0$). The cases in which ρ_i and ${}^{(3)}\mathcal{R}_i$ are, in general, not constant but become constant (even zero) only in an interval of the domain of r can be also understood as initial value functions of "hybrid" spacetimes obtained by matching a given LTB region (with ρ_i, ${}^{(3)}\mathcal{R}_i$ not constants) with a section of FLRW or Schwarzschild spacetimes in another part. These matchings can also be defined among various types of LTB (non-FLRW or non-Schwarzschild) regions (see [16], [17]). We will not examine these hybrid spacetimes in this paper (see [29]).

VI. LUMPS AND VOIDS IN THE INITIAL HYPERSURFACE.

A. Initial density lumps and voids.

The relation of ρ_i with $\langle\rho_i\rangle$ and $\Delta_i^{(m)}$ is straightforward. Consider the following auxiliary equations obtained by applying integration by parts to (37)

$$\begin{aligned} \rho_i \;-\; \langle\rho_i\rangle \;&=\; \frac{1}{Y_i^3}\int^r \rho_i{}'\,Y_i^3\,dr \\ \Delta_i^{(m)} \;&=\; \frac{\int^r \rho_i{}'\,Y_i^3\,dr}{\rho_i\,Y_i^3 - \int^r \rho_i{}'\,Y_i^3\,dr} \end{aligned} \tag{64}$$

In all intervals of r containing a SC, $\rho_i{}' \neq 0$ implies $\Delta_i^{(m)} \neq 0$, except at the SC itself where both $\rho_i{}'$ and $\Delta_i^{(m)}$ must vanish (from (50) and (50)). We still have $\Delta_i^{(m)} \neq 0$, even if ρ_i and/or $\rho_i{}'$ vanish in a subset of this domain that contains no SC. With the help of (37) and (64), we discuss below the cases with one and two symmetry centers. Unless specificaly mentioned otherwise, we assume that either $\rho_i' \geq 0$ or $\rho_i' \leq 0$ throughout the interval under consideration. The discussion below is illustrated in figures 3.

- One symmetry center. See figures 3a and 3b.

  In this case a density "lump" or "void" is characterized by ρ_i having a maximum/minimum at the center worldline $r = r_c$. Hence, for a lump or void, we have (from (64)) the following possible ranges of $\Delta_i^{(m)}$

$$\begin{aligned} &\text{initial lump:} \quad \rho_i{}' \;\leq\; 0, \qquad \rho_i \;\leq\; \langle\rho_i\rangle, \qquad \Rightarrow \qquad -1 \;\leq\; \Delta_i^{(m)} \;\leq 0, \\ &\text{initial void:} \quad \rho_i{}' \;\geq\; 0, \qquad \rho_i \;\geq\; \langle\rho_i\rangle, \qquad \Rightarrow \qquad \Delta_i^{(m)} \;\geq\; 0, \end{aligned} \tag{65}$$

  where the lower bound on $\Delta_i^{(m)}$ for a lump is $\Delta_i^{(m)} = -1$ if ρ_i vanishes for $r > r_c$ (from(41)).

- Two symmetry centers. See figures 3c and 3d.

  From (50), (51) and (52), all of Y_i, M, M', $\rho_i{}'$, Y_i, $\rho_i - \langle\rho_i\rangle$ and $\Delta_i^{(m)}$ must vanish at both SC, $r = r_{c_1}$ and $r = r_{c_2}$, with zeroes of the same order in $r - r_{c_1}$ and $r - r_{c_2}$. This means that there must exist a turning value $r = r^*$ in the open domain $r_{c_1} < r < r_{c_2}$ for which Y_i', M', $\rho_i{}'$ all have a common zero of the same order at $r = r^*$. Besides these conditions, ρ_i and Y_i must satisfy

$$M(r_{c_2}) \;=\; \frac{4\pi G}{3c^4}\int_{r_{c_1}}^{r_{c_2}} \rho_i Y_i^2 Y_i' dr = 0 \tag{66}$$

Therefore, for every $r = a$ in the open domain $r_{c_1} < r < r_{c_2}$ we have

$$\int_{r_{c_1}}^{a} \rho_i Y_i^2 Y_i' dr \;=\; -\int_{a}^{r_{c_2}} \rho_i Y_i^2 Y_i' dr \;=\; \int_{r_{c_2}}^{a} \rho_i Y_i^2 Y_i' dr \tag{67}$$

Since Y_i vanishes at both SC's, this means that, for whatever ρ_i we choose, the average $\langle \rho_i \rangle$ evaluated from one center (say $r = r_{c_1}$) to $r = a$ must be the same as that average evaluated from the other center ($r = r_{c_2}$). Also, following the usual interpretation of M as the "effective mass inside" a comoving layer r, this "effective mass" for the whole hypersurface (from $r = r_{c_1}$ ro $r = r_{c_2}$) is zero.

We have two possible regular configurations (see figures 3c and 3d), depending whether ρ_i is: (i) a local maximum at each center (each center is a density lump) and (ii) a local minimum at each center (each center is a density void). For each case, $\Delta_i^{(m)}$ vanishes at the centers, while (from (64)) and using the same arguments as in the case of one center, we have for the cases (a) and (b).

$$\begin{aligned} &\text{an initial lump in each center:} \qquad \rho_i \;\leq\; \langle \rho_i \rangle, \qquad \Rightarrow \qquad -1 \;\leq\; \Delta_i^{(m)} \;\leq 0, \\ &\text{an initial void in each center:} \qquad \rho_i \;\geq\; \langle \rho_i \rangle, \qquad \Rightarrow \qquad \Delta_i^{(m)} \;\geq\; 0, \end{aligned} \tag{68}$$

If allow $\rho_i{}'$ to change its sign in a given domain containing a SC, we obtain an initial density that can be associated with "density ripples" (see figure 6a). In this case we have $-1 \leq \Delta_i^{(m)} \leq 0$ for all r for which $\rho_i{}'$ is negative and $\Delta_i^{(m)} \geq 0$ for positive $\rho_i{}'$.

B. Initial curvature lumps and voids.

Unlike ρ_i, the intial 3-curvature ${}^{(3)}\mathcal{R}_i$ can be zero, positive, negative or change signs in any given domain of r. This makes the relation between ${}^{(3)}\mathcal{R}_i$, $\langle {}^{(3)}\mathcal{R}_i \rangle$, K and $\Delta_i^{(k)}$ more complicated than in the case of ρ_i. Also, the regularity conditions (48) and (54), as well as the distinction between the type of dynamics (parabolic, hyperbolic or elliptic), all involve specific choices of ${}^{(3)}\mathcal{R}_i$ and K but not of ρ_i and M.

The following auxiliary relation, analogous to (64), follows from integration by parts of (38)

$${}^{(3)}\mathcal{R}_i \;-\; \langle {}^{(3)}\mathcal{R}_i \rangle \;=\; \frac{1}{Y_i^3} \int_{r_c}^{r} {}^{(3)}\mathcal{R}_i{}' \, Y_i^3 \, dr, \tag{69}$$

In all intervals of r containing a SC, ${}^{(3)}\mathcal{R}_i' \neq 0$ implies $\Delta_i^{(k)} \neq 0$, except at the SC itself where both quantities vanish (from (50) and (50)). If ${}^{(3)}\mathcal{R}_i = 0$ for a domain of r containing a SC, then $\langle {}^{(3)}\mathcal{R}_i \rangle = K = 0$ and this domain is a parabolic region (or a parabolic solution if it is the full domain of r). However, we might have ${}^{(3)}\mathcal{R}_i = 0$ and/or ${}^{(3)}\mathcal{R}_i{}' = 0$ in an open subset of the domain of r containing no SC's without K or $\Delta_i^{(k)}$ vanishing. We look at various cases below. The discussion below is illustrated by figures 4, 5 and 6b.

- ${}^{(3)}\mathcal{R}_i > 0$ for a domain of r containing a SC.

  The relation between ${}^{(3)}\mathcal{R}_i$, $\langle {}^{(3)}\mathcal{R}_i \rangle$, $\mathcal{K}$ and $\Delta_i^{(k)}$ is analogous to that between ρ_i, $\langle \rho_i \rangle$, M and $\Delta_i^{(m)}$ (see figures 4a, 4b and 4c). Since $\langle {}^{(3)}\mathcal{R}_i \rangle$ and K are everywhere positive, the dynamics of the dust layers is elliptic.

  The results for the cases of curvature "lumps" or "voids"(sign of ${}^{(3)}\mathcal{R}_i'$) and/or when there is one or two centers are analogous to those discussed earlier for ρ_i:

$$\begin{aligned} &\text{curvature lumps:} \qquad {}^{(3)}\mathcal{R}_i \;\leq\; \langle {}^{(3)}\mathcal{R}_i \rangle, \qquad -\frac{2}{3} \;\leq\; \Delta_i^{(k)} \leq\; 0, \\ &\text{curvature voids:} \qquad {}^{(3)}\mathcal{R}_i \;\geq\; \langle {}^{(3)}\mathcal{R}_i \rangle, \qquad \Delta_i^{(k)} \geq\; 0, \end{aligned} \tag{70}$$

  where the minimal value $-2/3$ follows from $K > 0$ and from the regularity of the left hand side in (45). Notice that condition (48) is not trivialy satisfied. We examine below the cases with one and two SC's.

– One SC. (See figure 4a).

From (36) and (51), the functions Y_i and K vanish at the center and increase as $r \to r_{\max}$, but (48) requires that $K \leq 1$ for all the domain of r. Condition (54) can be avoided by selecting $Y_i = S_i\, r$ so that Y_i' never vanishes. Necessary and sufficient condition for complying with (48) and (49) are

$$ {}^{(3)}\mathcal{R}_i \;\to 0 \qquad \text{and} \qquad K \;=\; \frac{1}{2\,Y_i}\int_{r_{c_1}}^{r} {}^{(3)}\mathcal{R}_i\, Y_i^2\, Y_i'\, dr \;\to\; 1 \quad \text{as} \quad r \;\to\; r_{\max}, \tag{71} $$

so that $\ell_i \to \infty$ as $r \to r_{\max}$. The model examined in [5] is a particular case of this type of configuration.

– Two SC's. (See figures 4b and 4c).

In this case all the functions K, K', ${}^{(3)}\mathcal{R}_i - \langle {}^{(3)}\mathcal{R}_i\rangle$ and $\Delta_i^{(k)}$ must vanish at both centers. Also, ${}^{(3)}\mathcal{R}_i'$, $\langle {}^{(3)}\mathcal{R}_i\rangle'$, K' must all vanish for a value r^* in the open domain $r_{c_1} < r < r_{c_2}$ where Y_i' vanishes. In order to satisfy (48) and (54), the functions ${}^{(3)}\mathcal{R}_i$ and Y_i to be selected so that the following conditions hold

$$ \int_{r_{c_1}}^{r_{c_2}} {}^{(3)}\mathcal{R}_i\, Y_i^2\, Y_i'\, dr \;=\; 2\,K(r_{c_2})\,Y_i(r_{c_2}) \;=0, $$

$$ \frac{1}{2\,Y_i(r^*)}\int_{r_{c_1}}^{r^*} {}^{(3)}\mathcal{R}_i\, Y_i^2\, Y_i'\, dr \;=\; K(r^*) \;=1, \tag{72} $$

The graphs of ${}^{(3)}\mathcal{R}_i$, $\langle {}^{(3)}\mathcal{R}_i\rangle$, K and $\Delta_i^{(k)}$ are shown in figures 4 and qualitatively analogous to those of ρ_i, $\langle\rho_i\rangle$, M and $\Delta_i^{(m)}$ in figures 3. The function K must vanish at the SC's (like M) and comply with (72).

- ${}^{(3)}\mathcal{R}_i < 0$ for a domain of r containing a SC. (See figures 5a and 5b).

  In this case we have $\langle {}^{(3)}\mathcal{R}_i\rangle$ and $\mathcal{K}$ negative for all the domain of r, condition (48) holds trivialy and dust layers follow hyperbolic dynamics. However, the characterization of "lump" or "void" in terms of the sign of ${}^{(3)}\mathcal{R}_i'$ is the inverse to that when ${}^{(3)}\mathcal{R}_i$ is nonegative: lump and void are now respectively characterized by ${}^{(3)}\mathcal{R}_i' > 0$ and ${}^{(3)}\mathcal{R}_i < 0$. Besides this point, the range of values of $\Delta_i^{(k)}$ for lumps and is the same as for the non-negative case in (70).

- ${}^{(3)}\mathcal{R}_i$ changes sign but K and $\langle {}^{(3)}\mathcal{R}_i\rangle$ do not. (See figure 6b).

  Since $\langle {}^{(3)}\mathcal{R}_i\rangle$ and K are obtained from an integral involving ${}^{(3)}\mathcal{R}_i$ evaluated from a SC to a given r, it is quite possible to have situations in which ${}^{(3)}\mathcal{R}_i$ vanishes or pases from positive to negative (or viceverza) but $\langle {}^{(3)}\mathcal{R}_i\rangle$ and K remains positive (or negative) at least for an interval of the domain of r not containing a SC, so that the model remains elliptic or hyperbolic in this domain. The situation in which $\langle {}^{(3)}\mathcal{R}_i\rangle$ or K vanish for a given $r = r^*$ in an open domain of r that excludes a SC is qualitatively different and more complicated, since the dynamic evolution of dust layers (governed by (3) or (20)) passes from elliptic to parabolic or hyperbolic (or viceverza). This case will be examined in a separate paper [29].

VII. THE FUNCTION Γ, SHELL CROSSING SINGULARITIES AND BANG TIMES.

The function Γ defined in (22) is essential for calculating relevant quantities characterizing LTB solutions, such as ρ, Θ, σ, ${}^{(3)}\mathcal{R}$ and ψ_2 ((A1), (A2), (A3), (A5) and (21)). The exact functional form of Γ is also required in order to find the restrictions on initial conditions that fulfil the important regularity condition:

$$ \Gamma \;\geq\; 0 \quad \text{for} \quad \rho_i \;\geq\; 0 \quad \text{and} \quad K \;\neq\; 1, \tag{73} $$

with $\Gamma = 0$ only if $\rho_i = 0$ and/or $1 - K = 0$. This condition garantees that: (a) the metric coefficient g_{rr} is regular, (b) $\rho \geq 0$ for a given choice of $\rho_i \geq 0$ and (c) provides the necessary and/or sufficient restrictions on initial value functions in order to avoid shell crossing singularities (these conditions are summarized in Table 1). We show in this section that the conditions for avoiding these singularities based on (73) are equivalent to those found by Hellaby and Lake [15] (see also [16] and [17]).

The function Γ can be obtained in terms of y and the initial value functions μ, κ, $\Delta_i^{(m)}$, $\Delta_i^{(k)}$ by eliminating y'/y from an implicit derivation with respect to r of equations (25), (26), (27) and (31). For hyperbolic and elliptic

dynamics, Γ in terms of η follows from implicit derivation of (29) and (33), using (28), (32), (30) and (34) in order to eliminate η' in terms of y'/y. We provide below the most compact forms of this function for parabolic solutions (in terms of y) and for hyperbolic and elliptic solutions (in terms of η)

$$\Gamma \;=\; 1 \;+\; \Delta_i^{(m)} \;-\; \frac{\Delta_i^{(m)}}{y^{3/2}}, \qquad \text{parabolic,} \tag{74}$$

$$\Gamma \;=\; 1 \;+\; 3\,(\,\Delta_i^{(m)} - \Delta_i^{(k)}\,)\left[1 \;-\; \frac{P}{P_i}\right] \;-\; 3\,P\,[\,Q - Q_i\,]\left(\Delta_i^{(m)} - \frac{3}{2}\Delta_i^{(k)}\right), \qquad \text{hyperbolic and elliptic,} \tag{75}$$

with $P(\eta)$ and $Q(\eta)$ given by

- Hyperbolic dynamics

$$P(\eta) \;=\; \frac{\sinh\,\eta}{(\cosh\,\eta - 1\,)^2} \;=\; \frac{\sqrt{2\,+\,x\,y}}{(\,x\,y\,)^{3/2}},$$

$$Q(\eta) \;=\; \sinh\,\eta - \eta \;=\; \sqrt{x\,y\,(2 + x\,y\,)} \;-\; \operatorname{arccosh}\,(1 + x\,y), \tag{76}$$

$$P_i \;=\; P(\eta_i) \;=\; \frac{\sqrt{2+x}}{x^{3/2}}, \qquad\qquad Q_i \;=\; Q(\eta_i) \;=\; \sqrt{x\,(2+x)} \;-\; \operatorname{arccosh}\,(1+x),$$

$$\eta \;=\; \operatorname{arccosh}\,(\,1 + x\,y\,) \;\geq\; 0, \qquad \eta_i \;=\; \operatorname{arccosh}\,(\,1 + x\,) \;\geq\; 0, \qquad x \;\equiv\; \frac{|\kappa|}{\mu}, \tag{77}$$

- Elliptic dynamics

$$P(\eta) \;=\; \frac{\sin\,\eta}{(\,1 - \cos\,\eta)^2} \;=\; \frac{\sqrt{x\,y\,(2\,-\,x\,y\,)}}{(\,x\,y\,)^2} \;=\; \pm\frac{\sqrt{2\,-\,x\,y}}{(\,x\,y\,)^{3/2}},$$

$$Q(\eta) \;=\; \eta \;-\; \sin\,\eta \;=\; \arcsin\,(\,1 - x\,y\,) \;-\; \sqrt{x\,y\,(2 - x\,y\,)}, \tag{78}$$

$$P_i \;=\; P(\eta_i) \;=\; \frac{\sqrt{2-x}}{x^{3/2}}, \qquad\qquad Q_i \;=\; Q(\eta_i) \;=\; \arccos\,(1-x) \;-\; \sqrt{x\,(2-x)},$$

$$\eta \;=\; \arccos\,(\,1 - x\,y\,), \qquad 0 \;\leq\; \eta \;\leq\; 2\pi$$

$$\eta_i \;=\; \arccos\,(\,1 - x\,), \qquad 0 \;<\; \eta_i \;<\; \pi, \qquad\qquad x \;\equiv\; \frac{\kappa}{\mu}, \tag{79}$$

where all functions of η and η_i have been constructed with (30) and (34) and the gradients of the form μ'/μ and κ'/κ were eliminated in terms of $\Delta_i^{(m)}$ and $\Delta_i^{(k)}$ by means of equations (44), (45) and (46). Notice that the $\pm$ sign in (78) follows from the fact that $\sin\eta$ becomes negative in the collapsing phase ($\pi \leq \eta < 2\pi$), whereas $\sinh(\eta)$ is positive for all $\eta \leq 0$. It is possible to use (77) and (79) in order to transform Γ in (75) as a function of y instead of η, but the obtained expressions are more complicated than (75). Also, the form of $\Gamma = \Gamma(y, r)$ for elliptic solutions consists of two branches, making it very impractical for most purposes.

Since the central and shell crossing singularities are (in general) not simmultaneous with respect to t, the existence of regular initial hypersurfaces $t = t_i$ is not a trivial issue. Such hypersurface must avoid the coordinate locii of shell crossing and central singularities. The conditions for avoiding shell crossings will be obtained below, not just for $t = t_i$, but for all the time evolution, but assuming that the no-shell-crossing conditions have been met, the hypersurface $\mathcal{T}_i$ must still avoid the central singularity. The conditions for this can be given straight away as

$$t_i \;-\; t_{_{bb}} \;>\; 0, \quad \text{for expanding layers,}$$

$$t_i \;-\; t_{_{bb}} \;<\; 0, \quad \text{for collapsing layers.} \tag{80}$$

These regularity considerations provide an insight on the relation of the "bang time" $t_{_{bb}}$ with the initial value functions ρ_i, ${}^{(3)}\mathcal{R}_i$ and their corresponding average and contrast functions. From the forms of $t_{_{bb}}$ that will be obtained in this section and displayed in figures 7, the fact that $t'_{_{bb}} \neq 0$ leads to an r dependent "age difference" for the comoving observers, a difference whose maximal value is very sensitive to $\Delta_i^{(m)}$ and $\Delta_i^{(k)}$, and so to the ratios of maximal to minimal ρ_i and ${}^{(3)}\mathcal{R}_i$ (but not to local values ρ_i or ${}^{(3)}\mathcal{R}_i$). This feature is illustrated in figures 7.

The fulfilment of conditions (73), as well as a comparison with no-shell-crossing conditions of Hellaby and Lake [15], is examined below for the cases with parabolic, hyperbolic and elliptic dynamics.

A. Parabolic solutions.

From (74) and (73), shell crossing singularities are avoided if

$$(1+\Delta_i^{(m)})\, y^{3/2} \;-\; \Delta_i^{(m)} \;\geq\; 0 \qquad \Rightarrow \qquad y^{3/2} \;\geq\; \frac{\Delta_i^{(m)}}{1+\Delta_i^{(m)}}, \tag{81}$$

Therefore, necessary and sufficient conditions for avoiding shell crossings are

$$-\,1 \;\leq\; \Delta_i^{(m)} \;\leq\; 0, \qquad \rho_i \;\geq\; 0, \tag{82}$$

conditions implying that we have initial density lumps.

Notice that condition (82) will not hold, in general, for density voids ($\Delta_i^{(m)} \geq 0$). However, since $\Delta_i^{(m)}/(1+\Delta_i^{(m)}) \leq 1$ and given a choice of a regular $t = t_i$, condition (82) is satisfied for initial lumps or voids and an evolution free of shell crossings is always possible for all $y \geq 1$ (or $t \geq t_i$ in expanding configurations). This fact allows for a well posed intial value study of LTB parabolic solutions with density voids, a feature that has been exploited in papers ([6], [8]) dealing with LTB solutions in which shell crossings do occur, but their coordinate locus can be confined to earlier times $t_{_{bb}} < t < t_i$ (see figure 11a).

The no-shell-crossing conditions of Hellaby and Lake ([15], [16], [17]) for the parabolic case and for expanding layers are given by

$$\pm\, Y' \;\geq\; 0 \quad \Rightarrow \quad \{\pm M' \;\geq 0, \quad \pm\, c\, t'_{_{bb}} \;\leq\; 0\}, \tag{83}$$

where the $\pm$ sign accounts for the possibility that Y' might change sign regularly (only if M' vanishes). However, the equality of the signs of Y' and M' in (83) follows from (53) and and $m' = \rho Y^2 Y' = \rho_i Y_i^2 Y'_i$, and is already contained in (73). Regarding the sign of $t_{_{bb}}$ we have, from setting $y = 0$ in (25), the following expression for $t_{_{bb}}$

$$c\, t_{_{bb}} \;=\; c\, t_i \;\mp\; \frac{2}{3\sqrt{2\,\mu}}, \tag{84}$$

where the $\mp$ sign accounts for expanding $(-)$ or collapsing $(+)$ layers. In order to compare with (83), we consider $t'_{_{bb}}$ the case of expanding layers

$$c\, t'_{_{bb}} \;=\; \frac{1}{3\sqrt{2\,\mu}}\,\frac{\mu'}{\mu} \;=\; \frac{1}{\sqrt{2\,\mu}}\,\frac{Y'_i}{Y_i}\,\Delta_i^{(m)}, \tag{85}$$

This equation clearly shows that $t'_{_{bb}} \leq 0$ for $Y'_i \geq 0$ only occurs if $\Delta_i^{(m)} \leq 0$. Thus, the no-shell-crossing conditions of Hellaby-Lake (83) are equivalent to (82). However, we argue that phrasing these conditions in terms of ρ_i, Y_i and $\Delta_i^{(m)}$ is more intutive than to do it in terms of Y', M' and $t'_{_{bb}}$. The function Γ for a regular model with parabolic dynamics is qualitatively analogous to the plot displayed in figure 10a.

Given a choice of $t = t_i$, it is evident from (82) that the intial hypersurface avoids shell crossings, either for lumps or voids (as long as $\Delta_i^{(m)}$ is finite). Regarding the central singularity, the form of $t_{_{bb}}$ in (84) implies that conditions (80) are satisfied as long as μ does not diverge, a condition that is, in turn, satisfied as long as ρ_i and ρ'_i are finite. As shown by figure 8, selecting unphysical initial conditions associated with "bad" choices of ρ_i (diverging at the SC or for $r > r_c$ in a void) leads to a singular $\mathcal{T}_i$ for which (80) is violated. As shown by figures 7a and 7b (the parabolic case is analogous to the hyperbolic one), for reasonable initial value functions it is always possible to garantee that a regular hypersurface $t = t_i$ exists. In general, a "good" choice of M and $t_{_{bb}}$, complying with (83), will yield a "good" form of ρ_i and Y_i complying with (82) and (80), however, we feel that selecting a 'good' form for ρ_i is easier and more intuitive that choosing adequate forms for $t_{_{bb}}$ and M.

B. Hyperbolic solutions.

In order to examine the fulfilment of (73), we assume that $\rho_i \geq 0$ and ${}^{(3)}\mathcal{R}_i \leq 0$ and rewrite (75) as

$$\Gamma \;=\; 1 \;+\; 3\left[A\,\Delta_i^{(m)} \;-\; B\,\Delta_i^{(k)}\right] \;-\; \frac{3\,P}{P_i}\left[A_i\,\Delta_i^{(m)} \;-\; B_i\,\Delta_i^{(k)}\right], \tag{86}$$

$$A(\eta) \;=\; 1 \;-\; P(\eta)\,Q(\eta), \qquad B(\eta) \;=\; 1 \;-\; \frac{3}{2}\,P(\eta)\,Q(\eta), \qquad A_i \;=\; A(\eta_i), \quad B_i \;=\; B(\eta_i), \tag{87}$$

where $P(\eta)$ and $Q(\eta)$ are given by (76). The fulfilment of (73) obviously depends on the behavior of A, B and P in the full range $\eta \geq 0$. We have $P \geq 0$ with $P \to \infty$ as $\eta \to 0$, while in the same limit $A \to 2/3$ and $B \to 0$. Therefore,the following are necessary conditions for (73)

$$A_i\,\Delta_i^{(m)} \;-\; B_i\,\Delta_i^{(k)} \;\leq\; 0, \tag{88}$$

$$1 \;+\; 3\left[A\,\Delta_i^{(m)} \;-\; B\,\Delta_i^{(k)}\right] \;\geq\; 0, \tag{89}$$

However, A and B satisfy $0 < A \leq 2/3$ and $-1/2 < B \leq 0$ for all $\eta \geq 0$, with $A \to 0$ and $B \to 1/2$ as $\eta \to \infty$. The functions A_i and B_i are bounded by the same values. Further restrictions follow by inserting these limiting values into (88) and (89). This leads to the following necessary and sufficient conditions for an evolution free of shell crossings

$$\rho_i \;\geq\; 0, \qquad {}^{(3)}\mathcal{R}_i \;\leq\; 0, \qquad -1 \;\leq\; \Delta_i^{(m)} \;\leq\; 0, \qquad -\frac{2}{3} \;\leq\; \Delta_i^{(k)} \;\leq\; 0, \tag{90}$$

Since (88) and (89) imply (90) and the latter also implies the former, conditions (90) are, indeed, necessary and sufficient. Notice that, just as for parabolic solutions, shell crossings cannot be avoided (in general, see subsection VII D below) for positive contrast functions (initial density or 3-curvature voids). The functions Γ and ρ for a regular model with hyperbolic dynamics are shown in figures 10a and 10b.

The no-shell-crossing conditions of Hellaby and Lake ([15], [16], [17]) for the hyperbolic case and for expanding layers are given by

$$\pm\,Y' \;\geq\; 0 \quad \Rightarrow \quad \{\pm\,M' \;\geq 0, \quad \pm\,K' \;\leq 0, \quad \pm\,c\,t'_{_{bb}} \;\leq\; 0\}, \tag{91}$$

where, as in the parabolic solutions, the $\pm$ sign accounts for the possibility that Y' might change sign regularly and we have used (14) in order to translate a positive E (in the original LTB variables) into a negative K. As in the parabolic solutions, the condition that Y', Y_i' and M' must have the same sign follows from (53), $\rho_i \geq 0$ and $m' = \rho Y^2 Y' = \rho_i Y_i^2 Y_i'$. Opposite sign for Y' and K' follows from (45) and ${}^{(3)}\mathcal{R}_i \leq 0$ (bearing in mind that $K < 0$ for hyperbolic solutions). Regarding the sign condition on $t'_{_{bb}}$, we compute $t_{_{bb}}$ by setting $\eta = 0$ and $y = 0$ in equations (31) and (33), leading to

$$c\,t_{_{bb}} \;=\; c\,t_i \;\mp\; \frac{\mu\,Q_i}{|\kappa|^{3/2}} \;=\; c\,t_i \;\mp\; \frac{1}{\sqrt{|\kappa|}}\left[\left(1+\frac{2}{x}\right)^{1/2} - \frac{\operatorname{arccosh}(1+x)}{x}\right], \qquad x \;\equiv\; \frac{|\kappa|}{\mu} \tag{92}$$

where the $\pm$ sign accounts for expanding $(-)$ and collapsing $(+)$ layers. Considering expanding layers and the expression given in terms of η_i, we obtain

$$c\,t'_{_{bb}} \;=\; \frac{3Y_i'}{Y_i}\,\frac{\mu}{|\kappa|^{3/2}\,P_i}\left[A_i\,\Delta_i^{(m)} \;-\; B_i\,\Delta_i^{(k)}\right], \tag{93}$$

but, because of (88), the factor in square brackets must be negative or zero for all $\eta_i > 0$, thus implying that $t'_{_{bb}}$ and Y_i' must have opposite signs. Looking at the maximal and minimal values of A_i and B_i, together with (44) and (45) leads then to conditions (90). Therefore, Hellaby-Lake no-shell-crossing conditions are equivalent to (90).

Assuming that (88) and (89) hold, a regular $\mathcal{T}_i$ must satisfy conditions (80) in order to avoid the central singularity. Since the term in square brackets in (92) tends, respectively, to 0 and 1 as $x \to 0$ and $x \to \infty$, sufficient conditions for (80) to hold are that both μ and $|\kappa| > 0$ be finite everywhere. These conditions are satisfied if $|{}^{(3)}\mathcal{R}_i| > 0$ and ρ_i are finite. As with the parabolic case, conditions (80) are violated only with very unphysical initial conditions

that might also violate the no-shell-crossing conditions (see figures 7a and 7b), since diverging ρ_i and $|{}^{(3)}\mathcal{R}_i|$ can be associated with for voids with large values of $\Delta_i^{(m)}$ and $\Delta_i^{(k)}$. Hence, a regular hypersurfaces $\mathcal{T}_i$ always exist for physicaly reasonable intial conditions and a 'good' selection of functions M, $E=-K$, $t_{_{bb}}$ leads to 'good' forms of ${}^{(3)}\mathcal{R}_i$, ρ_i, Y_i. However, we argue again, that finding a 'good' choice of the latter is easier and more intuitive.

Shell crossing singularities will always emerge for initial conditions with density and/or 3-curvature voids (see figure 7b), however for reasonable initial conditions characterized by finite $\rho_i \geq 0$ and ${}^{(3)}\mathcal{R}_i \leq 0$, we must have finite $\mu > 0$ and $\kappa < 0$ in all $\mathcal{T}_i$ (see section VIII for examples). Thus, unless we choose pathological initial value functions as in figure 8, quantities like P_i and Q_i defined in (77) will be finite and non-zero, leading to $\Gamma \to 1-(3/2)\Delta_i^{(k)}$ as $\eta \to \infty$ asymptoticaly, therefore a regular evolution of intial voids is possible in the domain $t \geq t_i$ as long as $\Delta_i^{(k)} \leq 2/3$ (for expanding layers). An LTB model with initial voids and hyperbolic dynamics following this type of evolution is depicted in figure 11a.

C. Elliptic solutions.

As with the hyperbolic case, we assume that $\rho_i \geq 0$ and ${}^{(3)}\mathcal{R}_i \geq 0$ and rewrite (75) as

$$\Gamma \;=\; 1 \;+\; 3(\,\Delta_i^{(m)} \;-\; \Delta_i^{(k)}\,) \;-\; 3\,P\,Q\,\left(\,\Delta_i^{(m)} \;-\; \frac{3}{2}\Delta_i^{(k)}\right) \;-\; \frac{3P}{P_i}\,\left[\,A_i\,\Delta_i^{(m)} \;-\; B_i\,\Delta_i^{(k)}\,\right], \tag{94}$$

$$A_i \;=\; 1 \;-\; P_i\,Q_i, \qquad B_i \;=\; 1 \;-\; \frac{3}{2}\,P_i\,Q_i, \qquad P_i \;=\; P(\eta_i), \qquad Q_i \;=\; Q(\eta_i),$$

where $P(\eta)$ and $Q(\eta)$ are given by (78). Necessary and sufficient conditions for avoiding shell crossings can be obtained from (73) and (94). Following Hellaby and Lake [15], we explore the sign of the functions P and PQ near the big bang ($\eta \approx 0$) and near the big crunch ($\eta \approx 2\pi$). As $\eta \to 0$ we have $P \to +\infty$ and $PQ \to 2/3$, while $PQ \to 2\pi P \to -\infty$ as $\eta \to 2\pi$, therefore necessary conditions for $\Gamma \geq 0$ are

$$A_i\,\Delta_i^{(m)} \;-\; B_i\,\Delta_i^{(k)} \;\leq\; 0, \tag{95}$$

$$2\pi\,P_i\,\left(\,\Delta_i^{(m)} \;-\; \frac{3}{2}\Delta_i^{(k)}\right) + A_i\,\Delta_i^{(m)} - B_i\,\Delta_i^{(k)} \;=\; (2\pi - Q_i)\,P_i\,\left(\,\Delta_i^{(m)} \;-\; \frac{3}{2}\Delta_i^{(k)}\right) + \Delta_i^{(m)} - \Delta_i^{(k)} \;\geq\; 0, \tag{96}$$

Since the range of η_i is $0 < \eta_i \leq \pi$, we have $1/3 \leq A_i \leq 1,\ 0 \leq B_i \leq 1$ and $0 \leq Q_i \leq \pi$, a third necessary (but not sufficient) condition that follows from (95) and (96) is

$$\Delta_i^{(m)} \;-\; \frac{3}{2}\Delta_i^{(k)} \;\geq\; 0, \tag{97}$$

Following the arguments of Hellaby and Lake [15], we prove the sufficiency of (95) and (96) by assuming that

$$\begin{aligned} 1 \;+\; 3\left(\,\Delta_i^{(m)} \;-\; \Delta_i^{(k)}\right) \;&=\; 3\alpha\,(\eta_i)\,\left(\,\Delta_i^{(m)} \;-\; \frac{3}{2}\Delta_i^{(k)}\right), \\ \Delta_i^{(m)} \;-\; \frac{3}{2}\,\Delta_i^{(k)} \;&=\; -\frac{\beta(\eta_i)}{P_i}\,\left(A_i\,\Delta_i^{(m)} \;-\; B_i\,\Delta_i^{(k)}\right), \end{aligned} \tag{98}$$

for unspecified functions $\alpha(\eta_i)$, $\beta(\eta_i)$, so that

$$\Gamma \;=\; -\frac{A_i\,\Delta_i^{(m)} \;-\; B_i\,\Delta_i^{(k)}}{P_i}\,[\,\beta\,(\alpha \;-\; PQ\,) \;+\; P\,],$$

and the fulfilment of $\Gamma \geq 0$ requires (95) and $\beta \geq -P/(\alpha - PQ)$. However, from the forms of P and Q in (94), this latter condition can only be satisfied in the whole evolution range $0 < \eta < 2\pi$ if the functions α, β satisfy $\alpha \geq 2/3$ and $\beta \geq 1/(2\pi)$. Inserting these inequalities into (98) we obtain (96) together with $\Delta_i^{(m)} \geq -1$. Conditions (95) and (96) are then necessary and sufficient, but we still need to test the compatibility of these conditions with the signs of $\Delta_i^{(m)}$ and $\Delta_i^{(k)}$ (initial lumps or voids). Clearly, (95) is compatible with either $\Delta_i^{(m)} \leq 0$ and $\Delta_i^{(k)} \geq 0$ (density

lump and 3-curvature void) or with $\Delta_i^{(m)} \leq 0$ and $\Delta_i^{(k)} \leq 0$ (density and 3-curvature lumps). However, (96) is only compatible with the second choice. Therefore, the full set of necessary and sufficient conditions for avoiding shell crossing singularities are (97), together with

$$-\frac{2}{3} \;\leq\; \Delta_i^{(k)} \;\leq\; 0, \qquad -1 \;\leq\; \Delta_i^{(m)} \;\leq\; 0, \tag{99}$$

and the two inequalities (95) and (96) which can be combined into the single expression

$$2\,\pi\,P_i\,\left(\Delta_i^{(m)} \,-\, \frac{3}{2}\Delta_i^{(k)}\right) \;\geq\; P_i\,Q_i\,\left(\Delta_i^{(m)} \,-\, \frac{3}{2}\Delta_i^{(k)}\right) \,-\, \left(\Delta_i^{(m)} \,-\, \Delta_i^{(k)}\right) \;\geq\; 0, \tag{100}$$

A graphical representation of this condition is provided in figures 9a and 9b.

The no-shell-crossing conditions of Hellaby and Lake ([15], [16], [17]) for the elliptic case are given by

$$\pm\, Y' \;\geq\; 0 \quad \Rightarrow \quad \{\pm M' \geq 0, \quad \pm c\,t'_{_{bb}} \;\leq\; 0, \quad \pm c\,t'_{_{bb}} \;\geq\; \frac{-2\pi M}{K^{3/2}}\,\left(\frac{M'}{M} - \frac{3}{2}\frac{K'}{K}\right)\}, \tag{101}$$

where the $\pm$ sign accounts for the possibility that Y' might change sign regularly and (14) has been used. As in the parabolic and hyperbolic solutions, the condition that Y', Y_i' and M' must have the same sign follows from $\rho_i \geq 0$, (44), (53) and $m' = \rho\, Y^2 Y' = \rho_i\, Y_i^2 Y_i'$. The same sign for Y' and K' follows from $K \geq 0$, (45) and (88). Regarding the sign condition on $t'_{_{bb}}$, we compute $t_{_{bb}}$ by setting $\eta = 0$ and $y = 0$ in equations (26) and (29), leading to

$$c\,t_{_{bb}} \;=\; c\,t_i \;-\; \frac{\mu\,Q_i}{\kappa^{3/2}} \;=\; c\,t_i \;-\; \frac{1}{\sqrt{\kappa}}\,\left[\frac{\arccos\,(\,1\,-\,x\,)}{x} \;-\; \left(\frac{2}{x} - 1\right)^{1/2}\right],$$

$$0 \;\leq \kappa \;\leq 2\,\mu, \qquad x \;\equiv\; \frac{\kappa}{\mu}, \qquad 0 \;\leq\; x \;\leq\; 2 \tag{102}$$

We differentiate the term depending on η_i with respect to r

$$c\,t'_{_{bb}} \;=\; \frac{3Y_i'}{Y_i}\,\frac{\mu}{\kappa^{3/2}\,P_i}\,\left[\,A_i\,\Delta_i^{(m)} \;-\; B_i\,\Delta_i^{(k)}\,\right], \tag{103}$$

where A_i, B_i and P_i are the same functions given in (94). Comparing $t'_{_{bb}}$ above with (95), it is evident that the Hellaby-Lake conditions (101) involving $t'_{_{bb}}$ are the same as (95) and (96), and so can be reduced to (97) - (100) if one translates these conditions in terms of $\Delta_i^{(m)}$, $\Delta_i^{(k)}$ and η_i.

Assuming that (95) - (100) hold, a regular hypersurface $\mathcal{T}_i$ must satisfy both conditions (80) in order to avoid the central singularity (big bang and big crunch). The term in square brackets depending on x in (102) is bounded between 0 (as $x \to 0$) and $\pi/2$ (as $x \to 2$), also, we have $c(t_i - t_{_{bb}}) \to 2/(3\sqrt{2\mu})$ as $\kappa \to 0$. On the other hand, the big crunch time is $c\,t_{_{bc}} = c\,t_{_{bb}} + 2\pi\mu/\kappa^{3/2}$. Therefore, conditions (80) can only be violated if both κ and μ diverge but complying with $0 \leq \kappa/\mu \leq 2$, a situation that can be avoided if both μ and κ or ρ_i and ${}^{(3)}\mathcal{R}_i$ are finite. As shown by figures 7c, 7d and 7e, conditions (80) are satisfied for reasonable initial value functions, even in the cases displayed in 7d and 7e in which shell crossing occur. In general, a 'good' selection of functions M, $K = -E$, $t_{_{bb}}$ leads to 'good' forms of ${}^{(3)}\mathcal{R}_i$, ρ_i, Y_i and viceverza.

As with parabolic and hyperbolic solutions, initial conditions with density and/or 3-curvature voids lead, in general, to shell crossings but a regular evolution with these type of initial conditions is possible in the domain $t \geq t_i$. In order to illustrate this point, we consider Γ given by (75) and assume that $\rho_i \geq 0$ and ${}^{(3)}\mathcal{R}_i \geq 0$ are everywhere finite (in order to comply with (80)). Bearing in mind that: $3P(Q_i - Q) \geq -2$ and $1 - P/P_i \geq 0$ for $\eta \geq \eta_i$ (or $t \geq t_i$), a sufficient condition for $\Gamma \geq 0$ is given by

$$\Delta_i^{(k)} \;\leq\; \Delta_i^{(m)} \;\leq\; \frac{1}{2} \;+\; \frac{3}{2}\Delta_i^{(k)}, \tag{104}$$

This condition is illustrated graphicaly by figure 9c, leading to the model displayed in figure 11b, an elliptic LTB model with an initial density void that has a regular evolution for $t \geq t_i$.

D. Simmultaneous big bang.

An important special class of initial conditions is that characterized by a simmultaneous big bang: ie $y = 0$ taking place in a singular hypersurface marked by $t =$ constant. The conditions for a symmultaneous big bang readily follow by setting $t'_{_{bb}} = 0$ in (85), (93) and (103). Clearly, a symmultaneous big bang is incompatible with parabolic solutions, since $t'_{_{bb}} = 0$ in (85) implies $\Delta_i^{(m)} = 0$, but this case is the FLRW limit (see section V E). From (93) and (103), a symmultaneous big bang for hyperbolic and elliptic solutions implies the vanishing of the term in square brackets in the right hand sides of (86) and (94), that is

$$A_i\,\Delta_i^{(m)} \;=\; B_i\,\Delta_i^{(k)}, \tag{105}$$

so that Γ becomes

$$\Gamma \;=\; 1 \;+3\,\Big(A\,\Delta_i^{(m)} \;-\; B\,\Delta_i^{(k)}\Big) \tag{106}$$

The conditions for avoiding shell crossings depend on the forms of A and B given by (86) and (94). We assume that $\rho_i \geq 0$ and ${}^{(3)}\mathcal{R}_i \geq 0$ (elliptic) and ${}^{(3)}\mathcal{R}_i \leq 0$ (hyperbolic) are all finite and examine the hyperbolic and elliptic cases below:

- For hyperbolic solutions, both A and B are monotonously decreasing with $0 \leq A \leq 1/3$ and $-1/2 \leq B \leq 0$, while $A \to 1/3$, $B \to 0$ as $\eta \to 0$ and $A \to 0$, $B \to -1/2$ as $\eta \to \infty$. For the asymptotic limits, $\eta \approx 0$ and $\eta \to \infty$, we have respectively $\Gamma \approx 1 + \Delta_i^{(m)}$ and $\Gamma \approx 1 + (3/2)\Delta_i^{(k)}$. Since A_i and B_i have also opposite signs, these asymptotic limits, together with (105), lead to the following necessary conditions for avoiding shell crossings

$$\Delta_i^{(m)} \;\geq\; -1, \qquad \Delta_i^{(k)} \;\geq\; -\frac{2}{3}, \qquad \Delta_i^{(m)}\Delta_i^{(k)} \;\leq\; 0, \tag{107}$$

  The functions μ, κ, $\Delta_i^{(m)}$, $\Delta_i^{(k)}$ are related by (92) and (105), which can be expressed as

$$\Delta_i^{(k)} \;=\; \frac{x^{3/2} - \sqrt{2+x}\,\big[\,\sqrt{x}\,\sqrt{2+x} - \operatorname{arccosh}(1+x)\big]}{x^{3/2} - \frac{3}{2}\sqrt{2+x}\,\big[\,\sqrt{x}\,\sqrt{2+x} - \operatorname{arccosh}(1+x)\big]}\,\Delta_i^{(m)}, \tag{108}$$

$$\frac{1}{\sqrt{|\kappa|}}\,\left[\left(1+\frac{2}{x}\right)^{1/2} - \frac{\operatorname{arccosh}(1+x)}{x}\right] \;=\; c\,(t_i \;-\; t_{_{bb}}^{(0)}), \tag{109}$$

  where $t_{_{bb}}^{(0)} < t_i$ is the constant value of $t_{_{bb}}$ and $x = |\kappa|/\mu$.

- For elliptic solutions both A, B are non-negative, with $A \to 1/3$ and $B \to 0$ as $\eta \to 0$, while $B \to (3/2)A \to \infty$ as $\eta \to 2\pi$. By looking at the asymptotic behavior as $\eta \to 0$ and $\eta \to 2\pi$ and considering (105), we obtain the necessary conditions

$$\Delta_i^{(m)} \;\geq\; -1, \qquad \Delta_i^{(m)} \;-\; \frac{3}{2}\Delta_i^{(k)} \;\geq\; 0, \qquad \Delta_i^{(m)}\Delta_i^{(k)} \;\geq\; 0, \tag{110}$$

  As with the hyperbolic case, for $t_{_{bb}} = t_{_{bb}}^{(0)} < t_i$ a constant, and $x = \kappa/\mu$, the functions μ, κ, $\Delta_i^{(m)}$, $\Delta_i^{(k)}$ follow from (102) and (105)

$$\Delta_i^{(k)} \;=\; \frac{x^{3/2} - \sqrt{2-x}\,\big[\,\arccos(1-x) - \sqrt{x}\,\sqrt{2-x}\big]}{x^{3/2} - \frac{3}{2}\sqrt{2-x}\,\big[\,\arccos(1-x) - \sqrt{x}\,\sqrt{2-x}\big]}\,\Delta_i^{(m)}, \tag{111}$$

$$\frac{1}{\sqrt{\kappa}}\,\left[\frac{\arccos(\,1\,-\,x\,)}{x} \;-\; \left(\frac{2}{x}-1\right)^{1/2}\right] \;=\; c\,(t_i \;-\; t_{_{bb}}^{(0)}), \tag{112}$$

Since both sets of conditions (107) and (110) can be obtained by applying (105) to the no-shell-crossing conditions of the general cases with $t'_{_{bb}} \neq 0$ (ie (90), (99) and (100)), conditions (107) and (110) are necessary and sufficient.

A simmultaneous big bang greatly restricts the forms of μ and κ. Notice that it is not possible to obtain a closed form $\kappa = \kappa(\mu)$ from (109) or (112). Given a choice of ρ_i leading to μ and $\Delta_i^{(m)}$ from (23), (35) and (41), the constraints (109) or (112) must be solved numericaly in order to determine a very specific and unique form of κ for a given $t_{_{bb}}^{(0)}$. Having obtained κ numericaly, we can use it to construct $x = \kappa/\mu$ so that $\Delta_i^{(k)}$ can be computed from (108) or (111). The remaining functions, such as K and ${}^{(3)}\mathcal{R}_i$ follow from (43). This numerical evaluation was done in ploting κ and $\Delta_i^{(k)}$ in figures 12. A simmultaneous big bang leads to a much simpler expression for Γ, and correspondingly, to a significantly more lenient no-shell-crossing conditions (107) and (110). Since (107) and (110) are not incompatible with positive $\Delta_i^{(m)}$ or $\Delta_i^{(k)}$, these conditions can accomodate, besides lumps, some combinations of density and 3-curvature voids. Unfortunately, this particular class of initial conditions has a complicated description with the initial value functions that we have used. However, a simmultaneous big bang is a restrictive type of initial conditions, like for example to assume parabolic evolution (${}^{(3)}\mathcal{R}_i = 0$), or zero density or 3-curvature contrasts ($\Delta_i^{(m)} = 0$ or $\Delta_i^{(k)} = 0$). We tend to conclude that the small possibility of a dust configuration exactly attaining these very special sets of intial conditions makes them somehow unrealistic. Graphical examples of initial value functions and the function $y(t, r)$ for LTB models with a simmultaneous big bang and hyperbolic and elliptic dynamics are displayed in figures 12. The no-shell-crossing conditions obtained and discussed in this section are summarized in Table 1.

VIII. LTB MODELS 'A LA CARTE'.

The functions Y_i, ρ_i and ${}^{(3)}\mathcal{R}_i$ play the same role as the traditional variables M, E, $t_{_{bb}}$, that is, basic "building blocks" whose specification fuly determines any given LTB model. It is then entirely equivalent to work with the functions M, E, $t_{_{bb}}$ and the solutions of (3) (as is usualy done) or to use the initial value functions Y_i, ρ_i, ${}^{(3)}\mathcal{R}_i$ together with the solutions of (20). Given a choice of old variables M, $E = -K$, $t_{_{bb}}$, we can find ρ, ${}^{(3)}\mathcal{R}_i$, Y_i from equations (16), (17), (84), (92) and (102). For either set of variables it is always possible to use one of the functions in order to fix the radial coordinate, leaving the other two functions as free parameters. If the traditional variables are used in this process, then ρ and ρ_i can be computed from (4) and (16) once Y and Y' are known from the integration of (3). The alternative approach we suggest is to fix the radial coordinate with Y_i as in section V C, so that ρ_i and ${}^{(3)}\mathcal{R}_i$ become the free parameters to be used for computing μ, κ and the contrast functions, $\Delta_i^{(m)}$, $\Delta_i^{(k)}$ by means of equations (35) to (45). Next we can obtain Γ defined in (22) from the solutions of (20) (see section VII), leading to ρ (from (21)) and the remaining geometric and kinematic quantities provided in the Appendix: ${}^{(3)}\mathcal{R}$, σ, Θ, etc. The old functions M and $E = -K$ can be determined from (35) and (36), while $t_{_{bb}}$ can be obtained by setting $y = 0$ in equations (25) to (34) (see equations (84), (92) and (102) in section VII).

In the remaining of this section we provide a simple and practical, step-by-step, guideline on how to construct a given LTB model in terms of mathematicaly simple ansatzes for the new variables.[2]. We also show how the characteriztion of initial conditions as lumps or voids, as well as regularity conditions and relevant quantities (like y, Y, Γ, ρ, etc), can all be illustrated graphicaly by plots that can be easily generated by a standard Computer Algebra System (like Maple or Mathematica).

Step (1). Prescribe the initial value functions. Consider the following simple ansatzes

$$\rho_i \;=\; \bar{\rho}_i \,\frac{a_2 \;+\; a_1\, f^2}{1 \;+\; f^2}, \tag{113}$$

$${}^{(3)}\mathcal{R}_i \;=\; {}^{(3)}\bar{\mathcal{R}}_i \,\frac{b_2 \;+\; b_1\, f^2}{1 \;+\; f^2}, \tag{114}$$

$$Y_i \;=\; S_i\, f, \tag{115}$$

[2]These ansatzes are (obviously) not the most general initial conditions and are not based on any realistic observational data, we suggest them simply for illustrating the utility of the new variables. The curves plotted in all figures (except 6a and 8) were obtained from expressions derived in this section and generated with Maple.

where

- S_i is a constant characteristic length and $\bar{\rho}_i$, ${}^{(3)}\bar{\mathcal{R}}_i$ are suitable constant reference values of ρ_i, ${}^{(3)}\mathcal{R}_i$,
- $f = f(r)$ is a C^0 non-negative and adimensional function (see section V C) that satisfies:
  - $f(r_c) = 0$, where $r = r_c$ marks a SC, $f(r) > 0$ for all $r \neq r_c$.
  - $f \to \infty$ as $r \to r_{\max}$, with $r_{\max}$ defined by (49),
  - If there exist a "turning value" $r = r^*$ defined by $f'(r^*) = 0$, all radial derivatives of ρ_i, ${}^{(3)}\mathcal{R}_i$, μ, κ, K, M vanish at $r = r^*$.

and the adimensional real constants a_1, a_2, b_1, b_2 determine the following generic properties.

- Central and asymptotic values

  The central values $\rho_i(r_c)$, ${}^{(3)}\mathcal{R}_i(r_c)$ can be related to a_2, b_2 by

$$\rho_i(r_c) \;=\; a_2\,\bar{\rho}_i, \qquad {}^{(3)}\mathcal{R}_i(r_c) \;=\; b_2\,{}^{(3)}\bar{\mathcal{R}}_i, \tag{116}$$

  while in the case when there is a maximal value $r_{\max}$, the asymptotic values $\rho_i(r_{\max})$, ${}^{(3)}\mathcal{R}_i(r_{\max})$ relate to a_1, b_1 by

$$\rho_i(r_{\max}) \;=\; a_1\,\bar{\rho}_i \qquad {}^{(3)}\mathcal{R}_i(r_{\max}) \;=\; b_1\,{}^{(3)}\bar{\mathcal{R}}_i, \tag{117}$$

  Hence, we can consider the constants a_1, a_2, b_1, b_2 as comparative adimensional ratios of special values of ρ_i and ${}^{(3)}\mathcal{R}_i$ with respect to the reference values $\bar{\rho}_i$ and ${}^{(3)}\bar{\mathcal{R}}_i$, for example, values associated to a FLRW background (see further below). Numerical values of these constants used in all figures follow this interpretation, hence the curves display comparative values of the plotted quantities, say ρ_i, ${}^{(3)}\mathcal{R}_i$, etc, with respect to specific reference values (for example, with respect to central values if $a_1 = b_1 = 1$).

- Type of dynamics
  - Parabolic solutions: $b_1 = b_2 = 0$, so that ${}^{(3)}\mathcal{R}_i = \langle {}^{(3)}\mathcal{R}_i \rangle = \kappa = K = 0$.
  - If b_1, b_2 are both positive, the sign of ${}^{(3)}\mathcal{R}_i$ is given by the sign of ${}^{(3)}\bar{\mathcal{R}}_i$. We have elliptic or hyperbolic dynamics if ${}^{(3)}\bar{\mathcal{R}}_i \geq 0$ or ${}^{(3)}\bar{\mathcal{R}}_i \leq 0$.
  - Mixed dynamics: If b_1 and b_2 have different signs, $\langle {}^{(3)}\mathcal{R}_i \rangle$ and K might pass from positive to negative or viceverza (see figure 6b).

- Lumps and voids

  Since a_2/a_1 and b_2/b_1 are the ratios of central to asymptotic values of ρ_i and ${}^{(3)}\mathcal{R}_i$, the characterization of (113) and (114) as lumps or voids follows from these constants.

$$\begin{aligned} 0 \;\leq\; a_1 \;<\; a_2, \quad \text{density lumps,} \qquad & 0 \;\leq\; a_2 \;<\; a_1, \quad \text{density voids,} \\ 0 \;\leq\; b_1 \;<\; b_2, \quad \text{curvature lumps,} \qquad & 0 \;\leq\; b_2 \;<\; b_1, \quad \text{curvature voids,} \end{aligned} \tag{118}$$

  If $\rho_i(r_c) > 0$ and ${}^{(3)}\mathcal{R}_i(r_c) \neq 0$, we can identify $\bar{\rho}_i = \rho_i(r_c)$ and ${}^{(3)}\bar{\mathcal{R}}_i = {}^{(3)}\mathcal{R}_i(r_c)$ by setting $a_2 = b_2 = 1$. In this case, we have lumps if $a_1 < 1$, $b_1 < 1$ and voids if $a_1 > 1$, $b_1 > 1$. Of course, $\bar{\rho}_i$ and ${}^{(3)}\bar{\mathcal{R}}_i$ can also be identified with asymptotic values or with values associated with a FLRW background. For example, in a present day cosmological context ($t_i = t_0$, present cosmic time), we can identify $\bar{\rho}_i = \bar{\rho}_0$ and ${}^{(3)}\bar{\mathcal{R}}_i = {}^{(3)}\bar{\mathcal{R}}_0$ as constant values associated with a FLRW background at $t = t_0$. If we set $a_1 = b_1 = 1$, we can identify these constant parameters in terms of the observational parameters $\bar{\Omega}_0$, $\bar{H}_0$ of the FLRW background by

$$\frac{8\pi G}{3c^4}\,\bar{\rho}_0 \;=\; \bar{H}_0^2\,\bar{\Omega}_0, \qquad \frac{1}{6}\,{}^{(3)}\bar{\mathcal{R}}_0 \;=\; \bar{H}_0^2\,(\bar{\Omega}_0 - 1).$$

  The values of ρ_0 and ${}^{(3)}\mathcal{R}_0$ depend on r (from (113) and (114)), but the other parameters a_2, b_2 provide the ratio of the central and background values:

$$\frac{8\pi G}{3c^4}\,\rho_0(r_c) \;=\; \frac{8\pi G}{3c^4}\,\bar{\rho}_0\,a_2 \;=\; a_2\,\bar{H}_0^2\,\bar{\Omega}_0, \qquad \frac{1}{6}\,{}^{(3)}\mathcal{R}_0(r_c) \;=\; \frac{1}{6}\,{}^{(3)}\bar{\mathcal{R}}_0\,b_2 \;=\; b_2\,\bar{H}_0^2\,(\bar{\Omega}_0-1) \tag{119}$$

From this example, we clearly have a density lump/void if a_2 is greater/smaller than 1 and a 3-curvature lump/void if b_2 is greater/smaller than 1. In all figures we can assume that the numerical values of a_1, a_2 and b_1, b_2 can be interpreted as comparative adimensional ratios with respect to these FLRW reference values. If desired, units can be selected so that $\bar{\rho}_i$ and ${}^{(3)}\bar{\mathcal{R}}_i$, as well as terms like $4\pi G/c^4$ can be normalized to unity.

Step (2). Compute auxiliary variables: μ, κ, the volume averages and contrast functions. We need to evaluate the integrals (35) and (36) for free functions ρ_i,${}^{(3)}\mathcal{R}_i$, Y_i given by (113), (114) and (115). Let $\mathcal{M}$ and $\mathcal{K}$ be defined as

$$\mathcal{M} \;=\; 3\,\bar{\rho}_i\,S_i^3\int\frac{(a_2+a_1\,f^2)\,f^2\,f'\,dr}{1+f^2} \;=\; a_1\,f^3 \;+3\,(a_2-a_1)\,(f-\arctan\,f) \tag{120}$$

$$\mathcal{K} \;=\; 3\,{}^{(3)}\bar{\mathcal{R}}_i\,S_i^3\int\frac{(b_2+b_1\,f^2)\,f^2\,f'\,dr}{1+f^2} \;=\; b_1\,f^3 \;+3\,(b_2-b_1)\,(f-\arctan\,f) \tag{121}$$

From (23), (24) and (35)-(42) we obtain

$$M \;=\; \frac{4\pi G\,\bar{\rho}_i\,S_i^3}{3c^4}\,\mathcal{M}, \qquad \mu \;=\; \frac{4\pi G\,\bar{\rho}_i}{3c^4}\,\frac{\mathcal{M}}{f^3} \;=\; \frac{4\pi G}{3c^4}\,\langle\rho_i\rangle, \tag{122}$$

$$K \;=\; \frac{{}^{(3)}\bar{\mathcal{R}}_i\,S_i^2}{6\,f}\,\mathcal{K}, \qquad \kappa \;=\; \frac{{}^{(3)}\bar{\mathcal{R}}_i}{6}\,\frac{\mathcal{K}}{f^3} \;=\; \frac{1}{6}\,\langle{}^{(3)}\mathcal{R}_i\rangle, \tag{123}$$

$$\Delta_i^{(m)} \;=\; \frac{(a_2-a_1)\,\left[f^3+(1+f^2)\,(f-\arctan\,f)\right]}{(1+f^2)\,\mathcal{M}}, \tag{124}$$

$$\Delta_i^{(k)} \;=\; \frac{(b_2-b_1)\,\left[f^3+(1+f^2)\,(f-\arctan\,f)\right]}{(1+f^2)\,\mathcal{K}}, \tag{125}$$

Since μ is simply the average $\langle\rho_i\rangle$ in units cm^{-2}, while κ and $\langle{}^{(3)}\mathcal{R}_i\rangle$ differ by a factor of $1/6$, all plots displaying $\langle\rho_i\rangle$ and $\langle{}^{(3)}\mathcal{R}_i\rangle$ are qualitatively equivalent to plots displaying μ and κ. Numerical factors like ${}^{(3)}\bar{\mathcal{R}}_i/6$ or $4\pi G\bar{\rho}_i/c^4$ can always be absorbed into the numerical values of the constants a_1, a_2, b_1, b_2.

Step (3). Evaluate bang times.

- For parabolic dynamics, the bang time $t_{_{bb}}$ can be computed directly from inserting μ given by (122) into (84). For hyperbolic and elliptic dynamics with $t'_{_{bb}}\neq 0$ the bang time, $t_{_{bb}}$, is furnished by (92) and (102) in terms of κ and x. The variable $x=\kappa/\mu$ (or $x=|\kappa|/\mu$ in hyperbolic dynamics) follows directly from (122) and (123) as

$$x \;=\; \frac{c^4}{8\pi G}\,\frac{{}^{(3)}\bar{\mathcal{R}}_i}{\bar{\rho}_i}\;\;\frac{\mathcal{K}}{\mathcal{M}}, \tag{126}$$

  where we must consider $|{}^{(3)}\bar{\mathcal{R}}_i|$ for the hyperbolic case. The bang time $t_{_{bb}}$ follows directly from inserting κ from (123) and x from (126) into (92) and (102). This has been done in the plots displayed in figures 7.

- For the particular case with a simmultaneous big bang, the constraints (109) and (112) cannot be satisfied by μ and κ both having the forms (122) and (123). However, we can choose either one of these functions and find the other one from (108) to (112). We can choose ρ_i, μ, $\Delta_i^{(m)}$ from (113), (122) and (124) and then find $\kappa=\mu\,x$ and $\Delta_i^{(k)}$ by numericaly solving two of the equations (108) to (112). This is the way the plots of figure 12 were done.

Step (4). Verify fulfilment of regularity conditions

- The no-shell-crossing conditions (82), (90) and (99), involving only μ, $\Delta_i^{(m)}$ and $\Delta_i^{(k)}$, can be tested and illustrated directly with (122)-(125) (see Table 1 and figures 3, 4 and 5). However, there is no simple prescription on how to choose a_1, a_2, b_1, b_2 in order to comply with the no-shell-crossing condition (100) of elliptic solutions. In this case, it is convenient to express the functions P_i, Q_i in terms of $x = \kappa/\mu$ by means of (77), (78) and then in terms of a_1, a_2, b_1, b_2 and f by (126). As shown by figures 9a, 9b and 10c-e, it is not difficult to select the appropriate values of these parameters in order to comply with this regularity condition.

- Regularity conditions, such as (48) and (54), take the form

$$\frac{\mathcal{K}}{f} \;=\; b_1 f^2 \;+\; 3\,(b_2 - b_1)\left(1 - \frac{\arctan f}{f}\right) \;\leq\; \frac{6}{{}^{(3)}\bar{\mathcal{R}}_i\, S_i^2},. \tag{127}$$

  where the equality holds for every turning value such that $f' = 0$. Condition (127) places strong restrictions on the values of ${}^{(3)}\bar{\mathcal{R}}_i$ and ${}^{(3)}\mathcal{R}_i$ in models with elliptic dynamics.

Step (5). Choose a specific model. A wide variety of models with specific initial conditions can be constructed with (113), (114) and (115) by selecting suitable parameters $\bar{\rho}_i$, ${}^{(3)}\bar{\mathcal{R}}_i$, S_i and constants a_1, a_2, b_1, b_2 associated with comparative ratios with respect to reference values of ρ_i and ${}^{(3)}\mathcal{R}_i$ (central or FLRW values, as in (116), (117) or (119)), or to lumps/voids (from (118)), or to a given type of dynamics, while, following the discussion of section VI-C, simple forms of f can be selected for zero, one or two SC's. Ommiting the cases with mixed dynamics we have the following possibilities of fuly regular LTB models:

- Parabolic solutions with one SC: $b_1 = b_2 = {}^{(3)}\bar{\mathcal{R}}_i = 0,\ f = \tan r$. Central and maximal values of r are $r_c = 0$ and $r_{\max} = \pi/2$. Initial density profiles are as shown in figures 3a or 3b. Bang and shell crossing times are as shown in figures 7a and 7b. See figures 2a, 2b, 10a, 10b and 11a.

- Hyperbolic solutions with one SC: ${}^{(3)}\bar{\mathcal{R}}_i < 0,\ f = \tan r$. Central and maximal values of r are as in the parabolic case above. Initial density profiles are as shown in figures 3a or 3b. Initial 3-curvature profiles are as shown in figures 5a or 5b. Bang and shell crossing times are as shown in figures 7a and 7b. See figures 2a, 2b, 10a, 10b and 11a.

- Elliptic solutions with one SC's: ${}^{(3)}\bar{\mathcal{R}}_i > 0,\quad f = \tan r$. Central and maximal values of r are the same as the parabolic and hyperbolic cases above. Initial density profiles are as shown in figures 3a or 3b. There are no turning values r^*, but (71), and (127) must hold. Necessary and sufficient conditions for this are

$$b_1 \;=\; 0, \qquad \text{so that:} \qquad K \;\to\; 1 \quad \text{as} \quad r \to r_{\max} = \pi/2 \qquad \Rightarrow \qquad {}^{(3)}\bar{\mathcal{R}}_i \;= \frac{2}{b_2\, S_i^2}, \tag{128}$$

  therefore, the initial 3-curvature profiles must be as shown in figure 4a, clearly indicating that only curvature lumps are possible since ${}^{(3)}\mathcal{R}_i = 2/[S_i^2(1+\tan^2(r))] \geq 0$ and so, ${}^{(3)}\mathcal{R}_i' \leq 0$ for all r. The bang and shell crossing times are analogous to those displayed in figures 7a and 7b. A model with these characteristics but with $t_{_{bb}}' = 0$ was examined in [5]. See figures 2e, 2f, 9b, 10e and 10f.

- Elliptic solutions with two SC's: ${}^{(3)}\bar{\mathcal{R}}_i > 0,\quad f = \sin r$. Central values of r are $r_{c_1} = 0$ and $r_{c_2} = \pi$. There are no maximal values $r_{\max}$ and there is a turning value $r^* = \pi/2$. Initial density profiles must be as shown in figures 3c or 3d. Initial 3-curvature profiles must be as shown in figures 4b or 4c. Condition (127) must be satisfied with the equality holding for the turning value $r^* = \pi/2$ so that $f_* = \sin(\pi/2) = 1$. Hence the parameters b_1, b_2, S_i, ${}^{(3)}\bar{\mathcal{R}}_i$ are linked by the constraint

$$K(\pi/2) \;=\; 1 \qquad \Rightarrow \qquad b_1 \;+\; 3\,(\,b_2 \;-\; b_1\,)\left(1 \;-\; \frac{\pi}{4}\right) \;=\; \frac{6}{{}^{(3)}\bar{\mathcal{R}}_i\, S_i^2}, \tag{129}$$

  See figures 2c, 2d, 9a, 9c, 10c, 10d and 11b.

Since condition (127) cannot hold if $K \leq 0$ (parabolic and hyperbolic dynamics), surface layers necessarily emerge at turning points $f'(r^*) = 0$ for parabolic and hyperbolic solutions with two SC's. However, these configurations can

still be constructed with the expressions derived in this section.

Step (6). Evaluate and plot time dependent quantities.

Once all previous steps have been accomplished, we have all r dependent quantities in (25)-(34) fuly determined by (113)-(115) and (122)-(125) and (126), so that all relevant regularity conditions, such as (82), (90), (99), (100) and (127) can be tested (see Table 1). If this test is passed, we have fuly determined initial conditions for a regular evolution. We are ready to derive expressions for y (or Y from (18)) for all t beyond the initial hypersurface $\mathcal{T}_i$. For parabolic dynamics, we have $y = y(t, r)$ from (25). For hyperbolic and elliptic dynamics, we have either an implicit solution $t = t(r, y)$ (as in (26), (27) and (31)) or parametric solutions $[t = (r, \eta), y = y(r, \eta)]$ (as in (28), (29), (32) and (33)). The function Γ can be obtained as $\Gamma(t, r)$ in the parabolic case by inserting (25) into (74), then $\rho = \rho(t, r)$ follows from (21). For hyperbolic or elliptic dynamics we have $\Gamma = \Gamma(r, \eta)$ from (75) and $\rho = \rho(r, \eta)$ also follows from (21). All other time-dependent quantities, such as ${}^{(3)}\mathcal{R}$, σ, Θ and other invariant scalars given by equations (A1), (A2), (A3), (A5) and (A4), can be transformed as functions of (t, r), for parabolic dynamics, and as functions of (r, y) or (r, η), for hyperbolic and elliptic cases, by eliminating gradients like Y' and $\dot{Y}'$ in terms of Γ from (22) and then insterting the previously known $\Gamma(t, r)$ or $\Gamma(r, \eta)$. For hyperbolic and elliptic dynamics, we cannot obtain closed functional forms for the time dependent quantities in terms of (t, r). However, we can obtain 3d plots of y (and thus of all these expressions) in terms of (t, r), since they are all real functions defined over a domain contained in the plane (t, r), hence their image can be represented as parametric 3d plots of the form

$$y \;=\; [r,\, t(r,\eta),\, y(t,\eta)], \qquad \Gamma \;=\; [r,\, t(r,\eta),\, \Gamma(t,\eta)], \qquad \rho \;=\; [r,\, t(r,\eta),\, \rho(t,\eta)], \qquad \text{etc.}$$

where $\Gamma(r, \eta)$ is given by (75), while $\rho(r, \eta)$ follows from (21) once $y(r, \eta)$ and $\Gamma(r, \eta)$ are known (we are assuming, of course, that all r-dependent functions, such as ρ_i have already been determined by steps 1 to 5). These 3d plots can be easily generated with any general use Computer Algebra System, like Maple or Mathematica. The corresponding commands for plotting $y(t, r)$ are:

```
plot3d([r, t(r,eta), y(r,eta)], r = 0..Pi, eta = 0..2*Pi);                Maple,

ParametricPlot3D[{r, t[r, eta], y[r, eta]}, {r, 0, π}, {eta, 0, 2π}]      Mathematica,        (130)
```

where the parametric functions $t(r, \eta)$, $y(r, \eta)$ must be previously defined in each package and we considered in the example above the elliptic case with $f = \sin r$. The plotting commands for other quantities follow the same syntaxis. The reader familiar with either Maple or Mathematica (or other package) can, of course, embellish the plots by adding a wide variety of plot options concerning axes, fonts, labels, colors, etc. All curves and surfaces displayed in the figures were drawn with Maple, with those surfaces in figures 1, 2, 10 and 11 plotted using commands like that shown in (130). For the case of a simmultaneous big bang, we can still obtain simmilar 3d plots, but $t(r, \eta)$ and $y(r, \eta)$ need to be constructed with numerical values of either one of μ or κ.

ACKNOWLEDGMENTS

This work has been supported by the National University of Mexico (UNAM), under grant DGAPA-IN-122498.

---

[1] H. Bondi, *Mon. Not. R. Astr. Soc.* **107**, 410, (1947).
[2] W. Bonnor, *Mon. Not. R. Astr. Soc.* **159**, 261, (1974).
[3] W. Bonnor, *Mon. Not. R. Astr. Soc.* **167**, 55, (1974).
[4] W. Bonnor, *Class. Quantum Grav.*, **2**, 781, (1985).
[5] W. Bonnor, *Mon. Not. R. Astr. Soc.*, **217**, 547, (1985).
[6] W. Bonnor and A. Chamorro, *Ap. J.* **361**, 21, (1990).
[7] G.A. Burnet, *Phys. Rev.* D **43**, 1143, (1991).
[8] M.N. Cellerier, *Phys.Lett.*, **A249**, 37, (1998); *A. Ap.*, **353**, 63, (2000); *A. Ap.*, **362**, 840, (2000).
[9] A. Gromov, LANL preprints: gr-qc/9906041, gr-qc/9612038, gr-qc/9706013.
[10] S.W. Goode and J. Wainwright, *Phys. Rev.* , **D26**, 3315 (1982)

[11] G.F.R. Ellis and H. Van Elst, *Cosmological Models*, Cargèse Lectures, 1998, LANL preprint gr-qc/9812046.
[12] C. Hellaby, *Class. Quantum Grav.*, **4**, 635, (1987).
[13] C. Hellaby, *Gen. Rel. Grav.*, **20**, 1203, (1988).
[14] C. Hellaby and K. Lake, *Ap. J.* **282**, 1, (1984).
[15] C. Hellaby and K. Lake, *Ap. J.* **290**, 381, (1985). See *Ap. J.* **300**, 461, (1986) for erratum of this paper.
[16] N.P. Humphreys, *Observational analysis of the inhomogeneous universe*, Ph.D. thesis, University of Portsmouth, U.K., 1997.
[17] N.P. Humphreys and D.M. Matravers, *Regular spherical dust spacetimes*, LANL preprint gr-qc/9804023
[18] N.P. Humphreys, R. Maartens and D.M. Matravers, *Matching spherical dust solutions to construct cosmological models*, LANL preprint gr-qc/0009057, to appear *Gen. Rel. Grav.*
[19] N.P. Humphreys, R. Maartens and D.M. Matravers, *Ap. J.* **477**, 488, (1997).
[20] P.S. Joshi, *Phys.Rev.*, **D47**, 5357, (1993); *Class.Quant.Grav.*, **13**, 559, (1996); *Class.Quant.Grav.*, **13**, 3057, (1996); *Class.Quant.Grav.*, **14**, 1223, (1997); *Class.Quant.Grav.*, **16**, 41, (1999).
[21] D. Kramer, H. Stephani, M.A.H. MacCallum and E. Herlt, *Exact solutions of Einstein's field equations* (CUP, Cambridge, 1980).
[22] A. Krasiński, *Inhomogeneous Cosmological Models* (CUP, Cambridge, 1997).
[23] H. Liu, *Jou. Math. Phys.* **31**, 2459, (1990).
[24] F. Mena and R. Tavakol, *Class.Quant.Grav.*, **16**, 435, (1999).
[25] N. Mustapha, C. Hellaby, and G.f.R. Ellis, *Mon. Not. R. Astr. Soc.* **292**, 817, (1997).
[26] D, Pavón and R.A. Sussman, *Class. Quantum Grav.*, **18**, 1625, (2001).
[27] J. Silk, *Astr. Ap* **59**, 53, (1977).
[28] R. Sussman, *Class. Quantum Grav.*, **15**, 1759, (1999). See also: R. Sussman and J. Triginer, *Class. Quantum Grav.*, **16**, 167, (1999); R. A. Sussman and D. Pavón, *Phys. Rev.* D **60**, 104023 (1999).
[29] R.A. Sussman and L. Garcia Trujillo. In preparation.
[30] Y.B. Zel'dovich and L.P. Grishchuk, *Mon. Not. R. Astr. Soc.* **207**, 23, (1984).

TABLE OF NO-SHELL-CROSSING CONDITIONS.

In all cases ρ_i and ${}^{(3)}\mathcal{R}_i$ must be finite. Also: $\rho_i \geq 0$ and: ${}^{(3)}\mathcal{R}_i \geq 0$ (elliptic), ${}^{(3)}\mathcal{R}_i \leq 0$ (hyperbolic)		
$t'_{bb} \neq 0$		
Parabolic	$-1 \leq \Delta_i^{(m)} \leq 0$	eq. (82)
Hyperbolic	$-1 \leq \Delta_i^{(m)} \leq 0, \quad -\frac{2}{3} \leq \Delta_i^{(m)} \leq 0,$	eq. (90)
Elliptic	$-1 \leq \Delta_i^{(m)} \leq 0, \quad -\frac{2}{3} \leq \Delta_i^{(m)} \leq 0,$	eq. (99)
	$2\pi P_i \left(\Delta_i^{(m)} - \frac{3}{2}\Delta_i^{(k)}\right) \geq P_i Q_i \left(\Delta_i^{(m)} - \frac{3}{2}\Delta_i^{(k)}\right) - \left(\Delta_i^{(m)} - \Delta_i^{(k)}\right) \geq 0,$	eq. (100)
$t'_{bb} = 0$		
Hyperbolic	$-1 \leq \Delta_i^{(m)}, \quad -\frac{2}{3} \leq \Delta_i^{(k)}, \quad \Delta_i^{(m)}\Delta_i^{(k)} \leq 0,$	eq. (107)
Elliptic	$-1 \leq \Delta_i^{(m)}, \quad \Delta_i^{(m)} - \frac{3}{2}\Delta_i^{(k)} \geq 0, \quad \Delta_i^{(m)}\Delta_i^{(k)} \geq 0,$	eq. (110)
No-shell-crossings for $t \geq t_i$		
Hyperbolic and parabolic	Always possible	
Elliptic	$\Delta_i^{(k)} \leq \Delta_i^{(m)} \leq \frac{1}{2} + \frac{3}{2}\Delta_i^{(k)}$	eq. (104)

TABLE I. Summary of no-shell-crossing conditions discussed in section VII.

FIGURES.

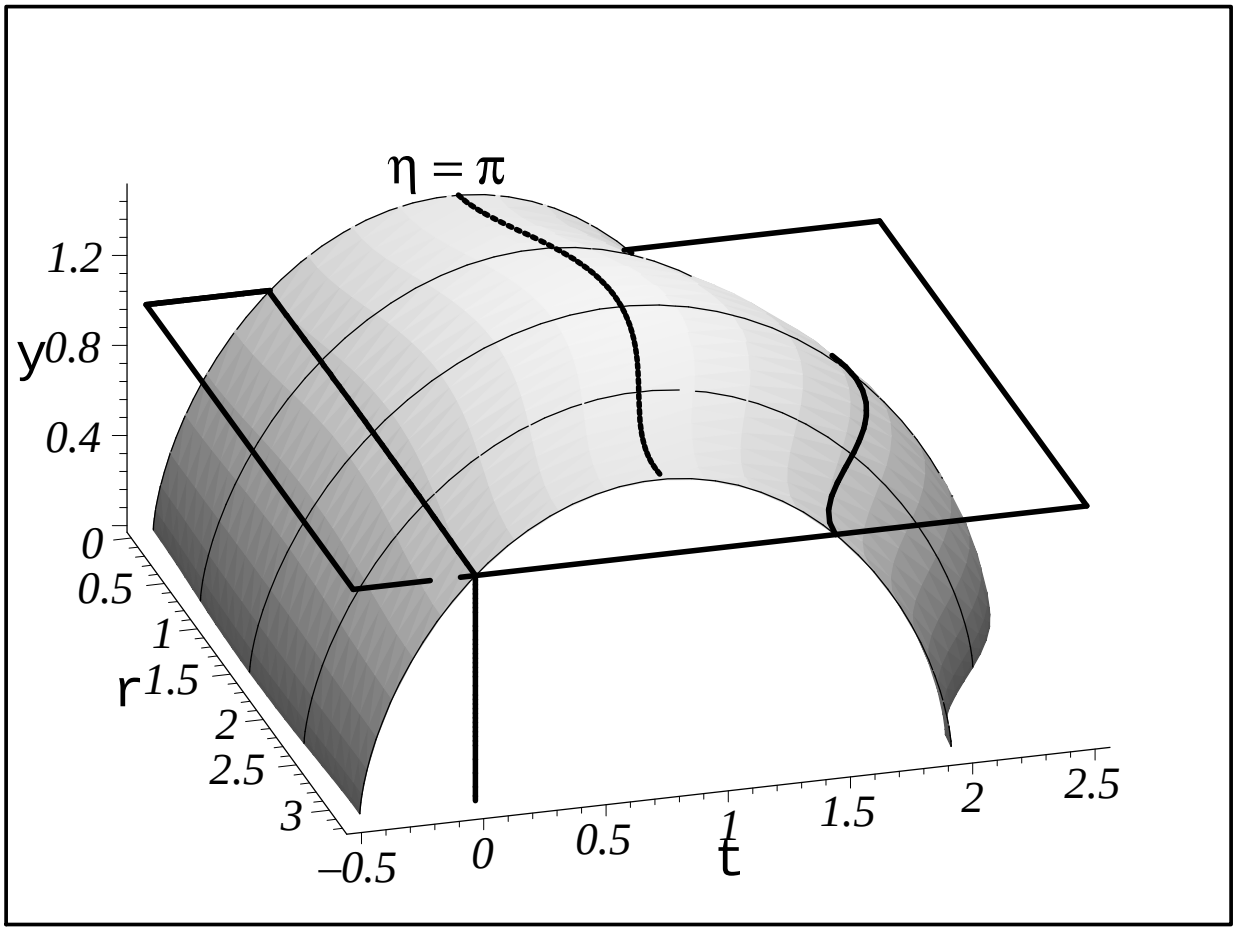

FIG. 1. Comoving layers in elliptic solutions. This figure displays $y(t,r)$ as a parametric 3-d plot $[r, t(r,\eta), y(r,\eta)]$ (see equation (130)) for a regular elliptic model with two SC's. We have considered as initial hypersurface $t_i = 0$ and all initial value functions were obtained from section VIII with $f = \sin r$ and $a_1 = 1$, $a_2 = 2$, $b_1 = 1$, $b_2 = 3$. Notice how the plane $y = 1$ coincides with $t = t_i = 0$ for all layers in the expanding phase, but in the collapsing phase the locuus $y = 1$ does not correspond to a single hypersurface of constant t. The figure also illustrates how the layers in the expanding and collapsing phases in elliptic dynamics are (in general) not time-symmetric with respect to any hypersurface of constant t. They are symmetric with respect to the hypersurface $\eta = \pi$ where $\dot{y} = 0$ (hypersurfaces of constant η do not coincide, in general, with those of constant t). These features also occur for other models with elliptic dynamics, such as models with one SC (see figure 2e) and models with a simmultaneous big bang (figure 12c).

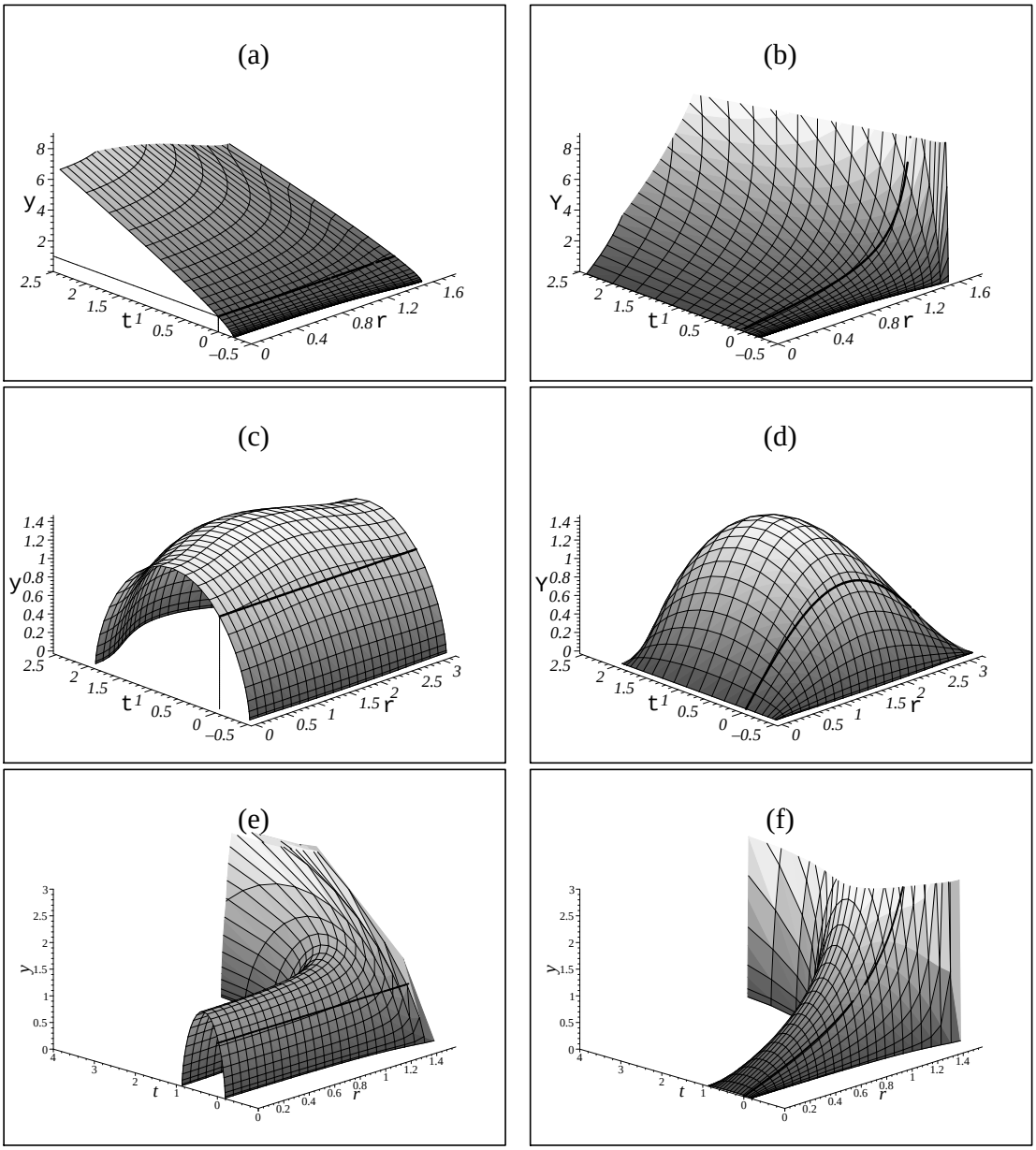

FIG. 2. Comoving layers in terms of $Y(t,r)$ and $y(t,r)$. These figures examine the difference between y and Y by looking at the functions $y(t,r)$ and $Y(t,r)$ obtained as parametric 3-d plots for three LTB models: one with hyperbolic dynamics and one SC (figures (a) and (b)), one with elliptic dynamics and two SC's (figures (c) and (d)) and one with elliptic dynamics and one SC (figures (e) and (f)). Figures (a), (c) and (e) depict $y(t,r)$, while $Y(t,r)$ is shown in figures (b), (d) and (f). Both y and Y have been plotted as suggested in (130), with initial value functions given in section VIII having the following parameters: figures (a) and (b) [$a_1 = 1$, $a_2 = 3$, $b_1 = 1$, $b_2 = 4$, $f = \tan r$], figures (c) and (d) [$a_1 = 1$, $a_2 = 2$, $b_1 = 1$, $b_2 = 3$, $f = \sin r$], figures (e) and (f) [$a_1 = 1$, $a_2 = 15$, $b_1 = 0$, $b_2 = 20$, $f = \tan r$]. The difference between y and Y emerges by comparing (a) vs (b), (c) vs (d) and (e) vs (f). In figures (b) and (f) we have $Y = 0$ for the central layer marked by $r = 0$, while figures (a) and (e) clearly illustrate the fact that $y > 0$ for this layer. The same happens in figures (c) and (d), but now also along the second SC at $r = \pi$. In figure (f) the function Y diverges along all hypersurfaces of constant t as r tends to the maximal value $r = \pi/2$ (since $f = \tan r \to \infty$). For the same model, as shown by figure (e), there are hypersurfaces of constant t, marked by $t < 1$, for which y remains everywhere bounded as $r \to \pi/2$. All these features reinforce the interpretation of y as a local "scale factor" for a given layer, in contrast with the curvature radius Y. The grids in the figure correspond to hypersurfaces of constant r (comoving layers) and of constant η. Notice how the latter do not coincide (in general) with hypersurfaces of constant t. The initial hypersurface, marked by $t = t_i = 0$, is shown as a thick line in figures (a), (c) and (e). Notice that $y = 1$ for all layers at $t = 0$. The thick curves shown in figures (b), (d) and (f) are the "profile" of $Y_i = Y(t_i, r)$ that corresponds to f in each case.

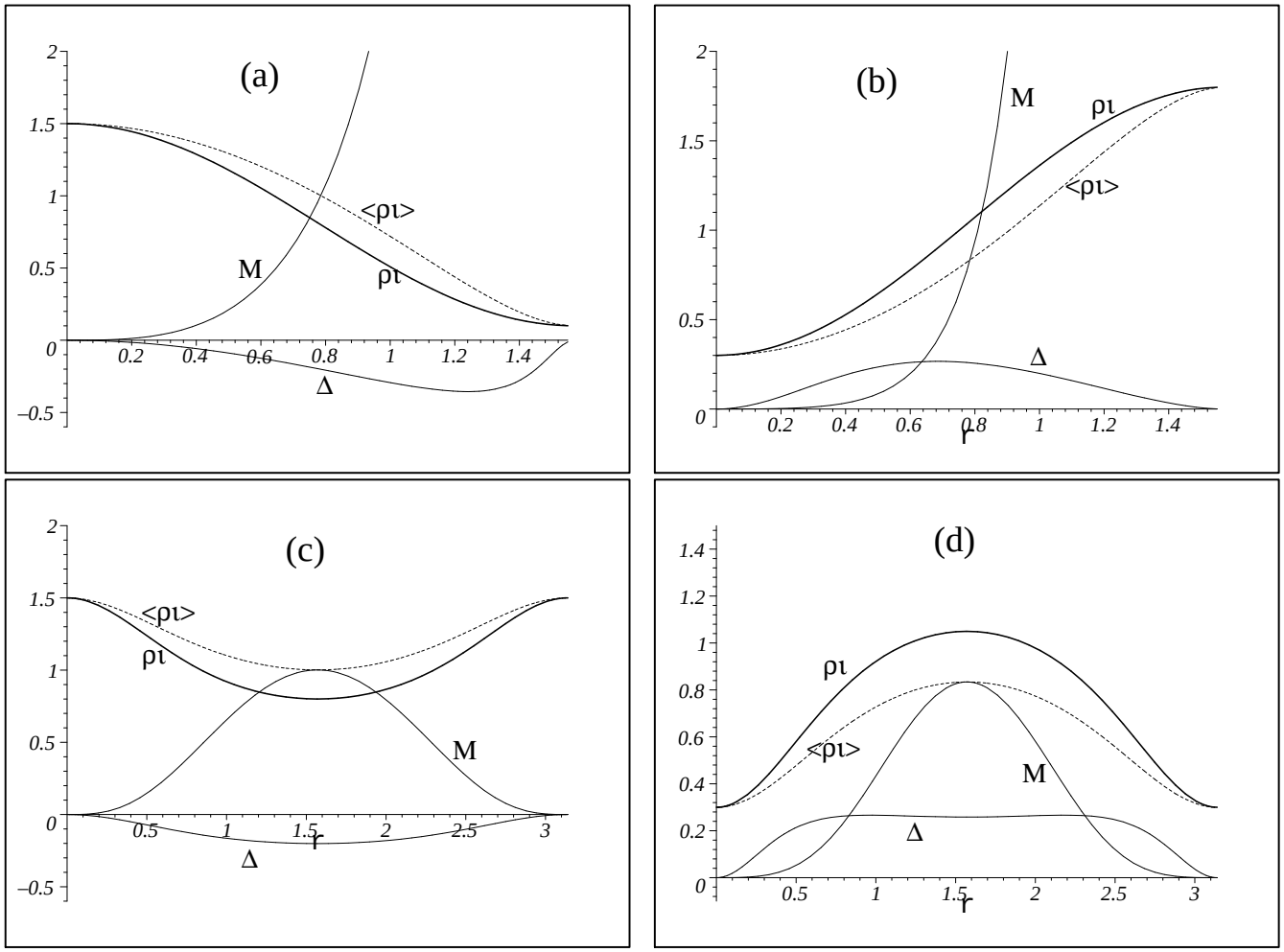

FIG. 3. Initial density lumps and voids. Initial value functions ρ_i (thick curve), $\langle\rho_i\rangle$ (dotted curve), M and $\Delta_i^{(m)}$ (marked by the symbol Δ) are depicted for a hypersurface $\mathcal{T}_i$ with one SC (figures (a) and (b)) and two SC's (figures (c) and (d)). Figures (a) and (c) depict initial density lumps in which ρ_i is a local maximum at the SC's, while figures (b) and (d) correspond to voids in which ρ_i is a local minimum at the SC's. These functions were obtained from section VIII with parameters: $[a_1 = 0.1,\ a_2 = 1.5]$ for the lumps ((a) and (c)) and $[a_1 = 1.8,\ a_2 = 0.3]$ for the voids ((b) and (d)), with $f = \tan r$ in (a) and (b) and $\sin r$ in (c) and (d). Notice that $\langle\rho_i\rangle \geq \rho_i$ for lumps ((a) and (c)) and $\langle\rho_i\rangle \leq \rho_i$ for voids ((a) and (c)), hence $\Delta_i^{(m)}$ is negative for lumps and positive for voids, clearly illustrating how the sign of this contrast function characterizes the nature of the inhomogeneity in density along an initial hypersurface $\mathcal{T}_i$. In all cases M vanishes at the centers and $M' = 0$ at the turning value $r = r^* = \pi/2$ (in (c) and (d)), showing the same qualitative behavior for lumps or voids. Since the type of dynamics (parabolic, elliptic or hyperbolic) depends on ${}^{(3)}\mathcal{R}_i$ and not on ρ_i, the initial density profiles in (a) and (b) can correspond to any dynamics (see figures 4a, 5a and 5b). Regular LTB models (without surface layers) having the initial density profiles shown (c) and (d) must have the 3-curvature profiles with two SC's shown in figures 4b and 4c.

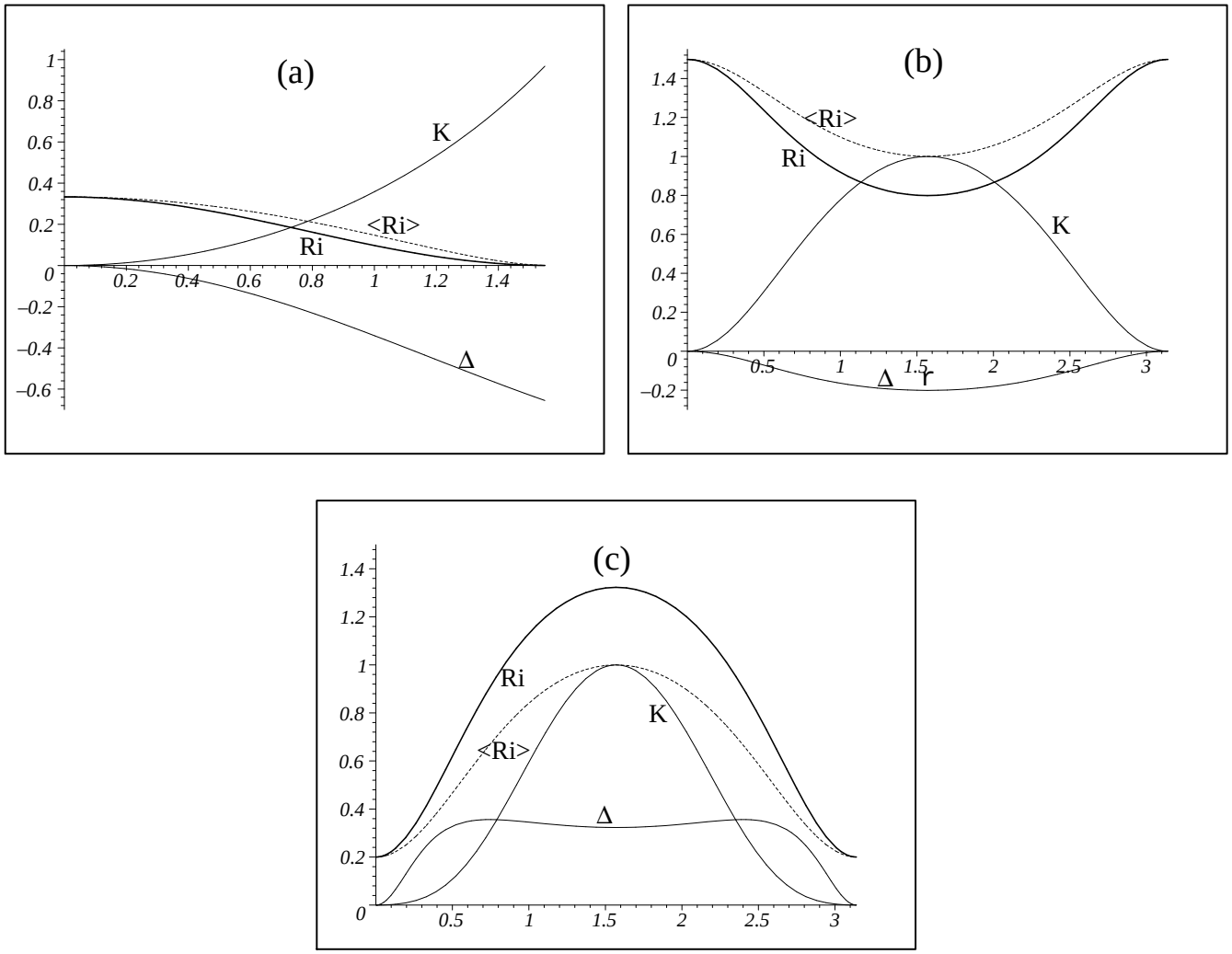

FIG. 4. Initial lumps and voids of positive 3-curvature. The figures display initial value functions ${}^{(3)}\mathcal{R}_i$ (thick curves), $\langle {}^{(3)}\mathcal{R}_i \rangle$ (dotted curves), K and $\Delta_i^{(k)}$ (marked by the symbol Δ) associated with an initial 3-curvature profile with ${}^{(3)}\mathcal{R}_i > 0$, hence the dynamics is necessarily elliptic. Lumps or voids of the 3-curvature correspond to local maxima or minima of ${}^{(3)}\mathcal{R}_i$ at the SC's. Figure (a) shows the case of a 3-curvature lump with one SC ($f = \tan r$), while (b) and (c) respectively depict lumps and voids with two SC's ($f = \sin r$). Models with elliptic dynamics must comply with regularity conditions (48) and (54). For the functions of section VIII these conditions are equivalent to (127), hence the constant parameters b_1, b_2, S_i and ${}^{(3)}\bar{\mathcal{R}}_i$ must satisfy condition (128) for the case in (a) and condition (129) for the cases in (b) and (c). Notice that $K \to 1$ as $r \to \pi/2$ in (a) and $K(\pi/2) = 1$ in (b) and (c). The contrast function $\Delta_i^{(k)}$ is positive/negative for voids/lumps, while K vanishes at the SC's and has the same qualitative behavior for lumps and voids. The initial density profiles that match the configuration in (a) is either one of those depicted by figures 3a or 3b, while for the cases in (b) and (c) it would be either one shown in figures 3c or 3d.

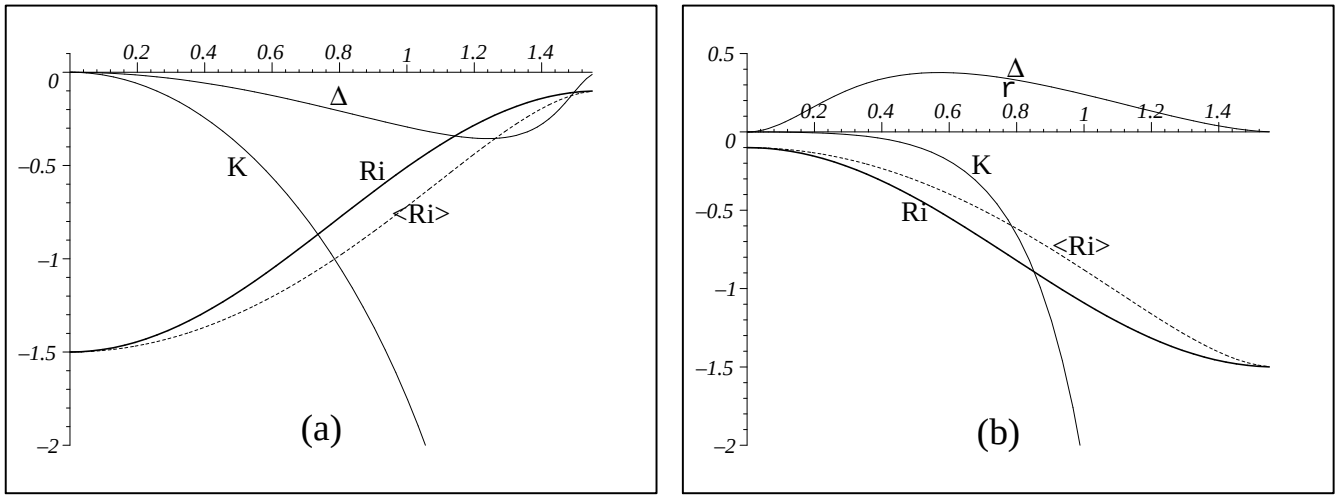

FIG. 5. Initial lumps and voids of negative 3-curvature. These figures show ${}^{(3)}\mathcal{R}_i$ (thick curves), $\langle {}^{(3)}\mathcal{R}_i\rangle$ (dotted curves), K and $\Delta_i^{(k)}$ (marked by the symbol Δ), defined by (24), (36), (40) and (42), for the case of negative 3-curvature ${}^{(3)}\mathcal{R}_i \leq 0$, corresponding to hyperbolic dynamics. Figure (a) displays a lump and figure (b) a void. Notice that now lumps/voids are characterized by local minima/maxima of ${}^{(3)}\mathcal{R}_i$ at the SC (the pictures depict only the case with one SC). The plots were obtained with equations (114), (123) and (125), with $f = \tan r$, ${}^{(3)}\bar{\mathcal{R}}_i = -1$, $S_i = 1$, $b_1 = 0.1, b_2 = 1.5$ in (a) and $b_1 = 1.5$, $b_2 = 0.1$ in (b). The corresponding initial density profile for these figures would be either one of those shown in figures 3a or 3b.

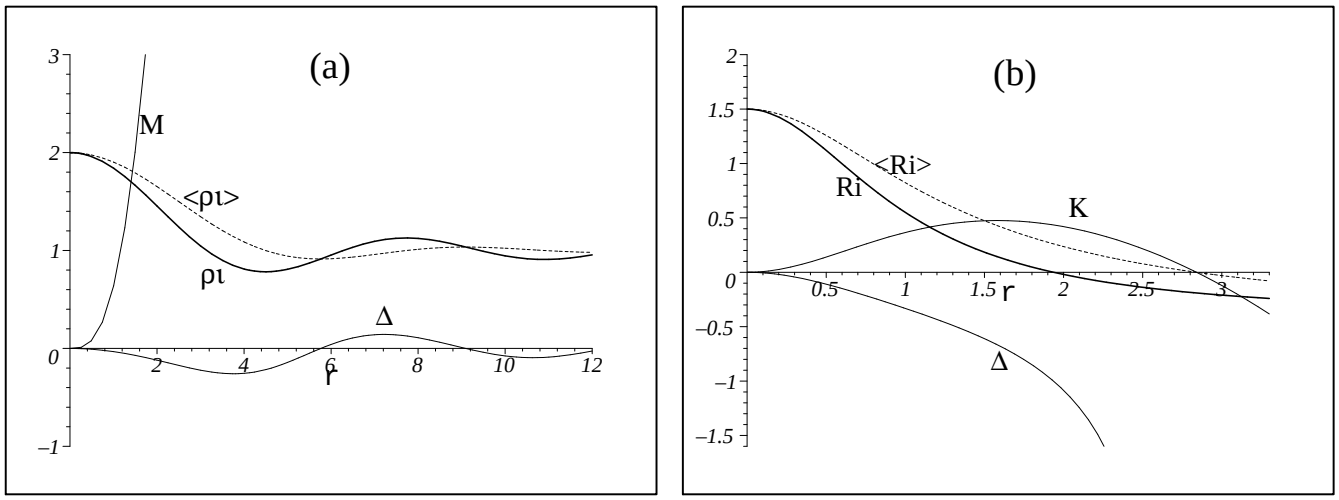

FIG. 6. Other initial conditions. Figure (a) depicts the case where ρ_i has many local maxima and minima, so that ρ_i' changes sign many times (ie "ripples"), then the contrast function $\Delta_i^{(m)}$ changes sign at each turning value. The function used in this example is $\rho_i = \bar{\rho}_i(1 + \sin r/r)$ with $\bar{\rho}_i = 1$ and there is only one SC. From (48), (54) and the no-shell-crossing conditions derived in section VII and summarized in Table 1, such configurations must have elliptic dynamics (with $K = 1$ at each turning value) and might be very prone to develop shell crossings. Figure (b) displays ${}^{(3)}\mathcal{R}_i$ (thick curve), $\langle {}^{(3)}\mathcal{R}_i\rangle$ (dotted curve), K and $\Delta_i^{(k)}$, defined by (24), (36), (40) and (42), for a 3-curvature lump in which an initialy positive ${}^{(3)}\mathcal{R}_i$ becomes negative. The functions $\langle {}^{(3)}\mathcal{R}_i\rangle$ and K also change sign (change from elliptic to hyperbolic dynamics). Notice that the passage from elliptic to hyperbolic dynamics does not coincide with the zero of ${}^{(3)}\mathcal{R}_i$, hence there is a range of r in which ${}^{(3)}\mathcal{R}_i < 0$ but $\langle {}^{(3)}\mathcal{R}_i\rangle$ and K are still positive. The plots were obtained with equations (114), (123) and (125) with $f = r$, ${}^{(3)}\bar{\mathcal{R}}_i = 1$, $S_i = 1$, $b_1 = -0.4$ and $b_2 = 1.5$. Since $\langle {}^{(3)}\mathcal{R}_i\rangle$ and K vanish at the value of r marking the transition from elliptic to hyperbolic dynamics, we have (because of (43)) $\Delta_i^{(k)} \to -\infty$ for this value of r.

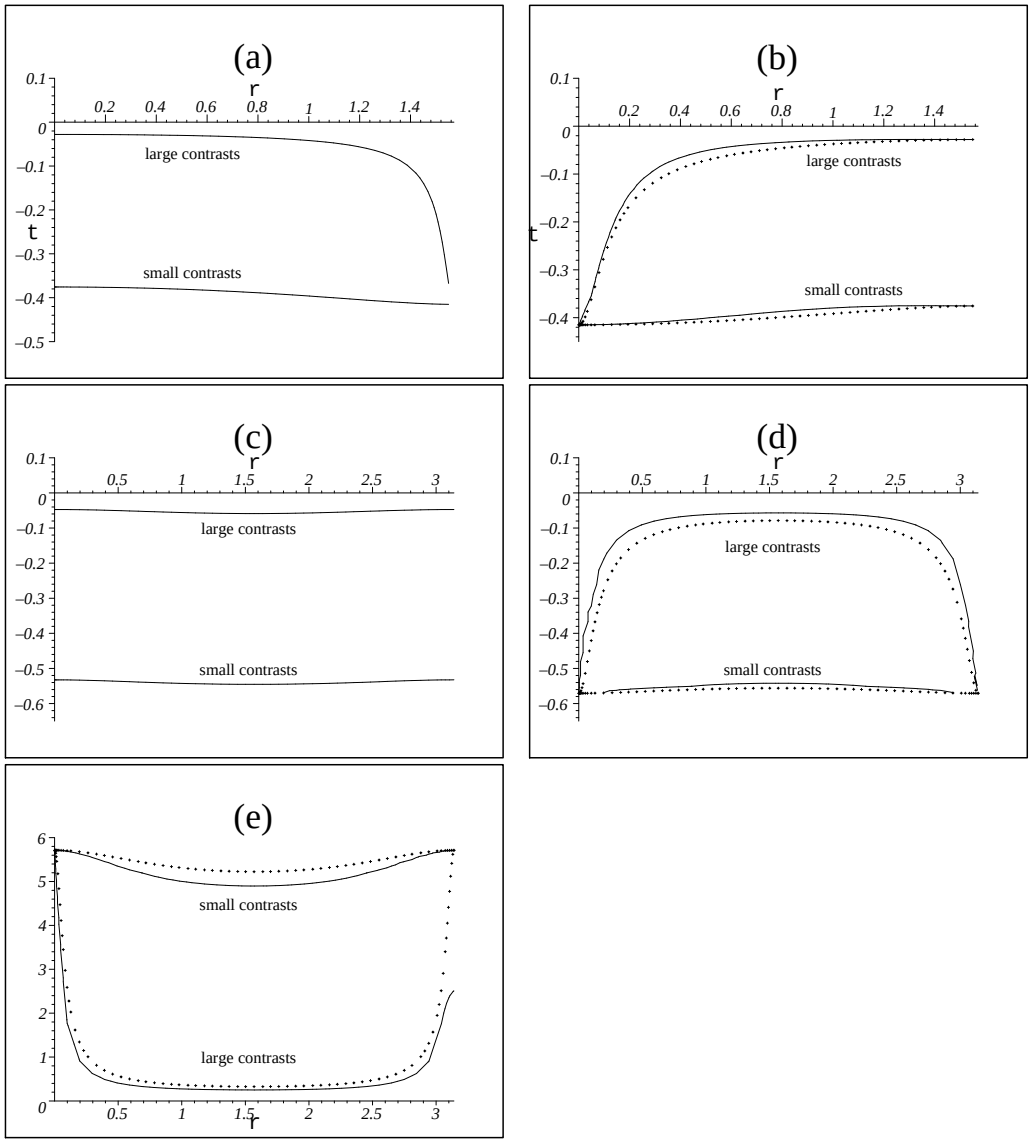

FIG. 7. Bang and shell crossing times. The figures display plots of the bang time function $t_{bb}(r)$, equivalent to displaying the locus of the central singularity ($y = 0$) in the coordinate patch (t, r). The locus of the shell crossing ($\Gamma = 0$) singularity is also displayed in those cases that exhibit this feature (solid curves in figures (b), (d) and (e)). Figures (a) and (c) correspond to initial density and 3-curvature lumps with hyperbolic dynamics and one SC (figure (a)) and elliptic dynamics and two centers (figure (c)). Configurations with initial voids are shown in figures (b) (with hyperbolic dynamics), (d) and (e) (elliptic dynamics, expanding and collapsing phases). All the plots were made with initial value functions obtained from section VIII, with $f = \tan r$ and $f = \sin r$ for hyperbolic and elliptic dynamics. Lumps with "small contrasts" are characterized by $a_1 = b_1 = 1$, $a_2 = 1.2$, $b_2 = 1.3$, while "large contrasts" correspond to $a_1 = b_1 = 1$, $a_2 = 200$, $b_2 = 300$. The same values characterize voids, exchanging a_1, b_1 for a_2, b_2. Notice how configurations with small contrasts are "older", in the sense of larger time lapse between t_{bb} and $t_i = 0$. Also, this "age" varies with r due to the dependence of t_{bb} on r, this variation is larger for large contrasts and hyperbolic dynamics (figures (a) and (b)), while for small contrasts and elliptic dynamics it is almost insignificant. In figures (b), (d) and (e), the curve of t_{bb} is marked by crosses while those of shell crossings are solid lines. Comoving observers ($r = \text{const.}$) in all these cases cannot avoid the shell crossings, but in the hyperbolic case (figure (b)) this singularity is confined to the past of the initial hypersurface $t_i = 0$. As shown by figures (d) and (e), the shell crossing singularity might exhibit two branches for elliptic dynamics, unless we choose initial conditions satisfying (104) as shown in figures 9c and 11b. The locii of singularities in cases with parabolic dynamics is qualitatively analogous to those of hyperbolic dynamics shown in (a) and (b).

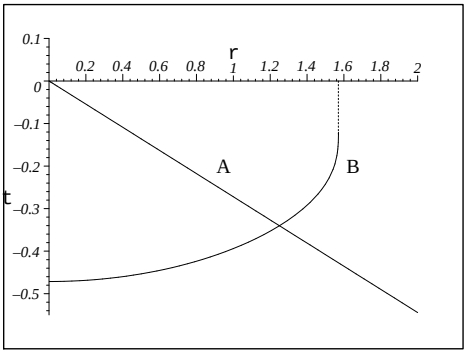

FIG. 8. Ill-suited initial value functions. The figure displays the bang time t_{bb} for "bad" choices of the initial value function ρ_i. The initial hypersurface $\mathcal{T}_i$ is marked by $t = 0$, we have chosen $Y_i \propto r$ and ${}^{(3)}\mathcal{R}_i = 0$ (parabolic dynamics), so that t_{bb} is given by (84). The curve "A" correponds to $\rho_i \propto 1/r$, a form that is singular at the SC ($r = 0$), hence $\mathcal{T}_i$ is also singular at $r = 0$ (it is intersected by t_{bb} at $r = 0$). The curve "B" corresponds to $\rho_i \propto 1/\cos r$, diverging as $r \to \pi/2$. In this case $\mathcal{T}_i$ is singular at $r = \pi/2$ (it is intersected by t_{bb}). For this choice of ρ_i we have a void with infinite contrast and so shell crossings necessarily emerge. Notice (from figure 7) that $\mathcal{T}_i$ is perfectly regular for all initial value functions obtained from the expressions of section VIII. We need to select truly pathological initial value functions in order to have a singular $\mathcal{T}_i$.

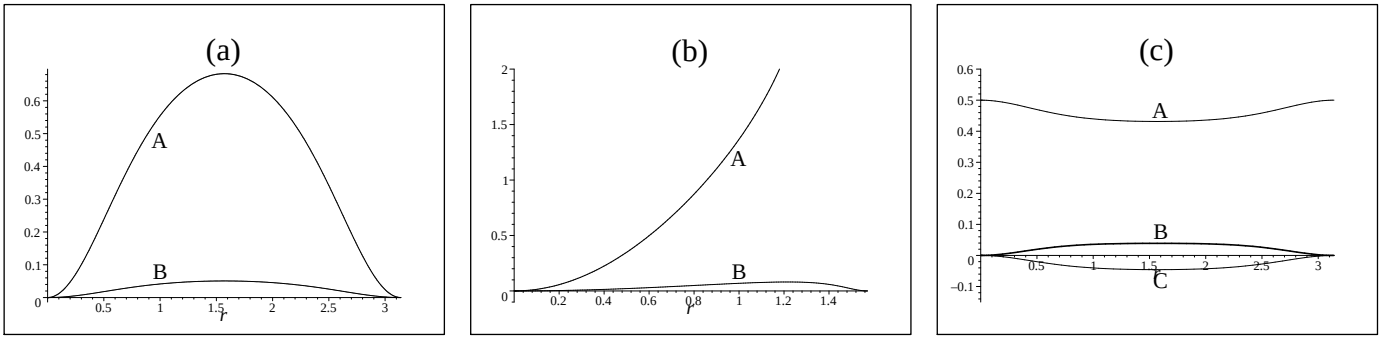

FIG. 9. Testing initial conditions for regularity. A graphical representation is provided in (a) and (b) for the no-shell-crossing condition of elliptic dynamics (100). Figure (c) ilustrates the condition (104) allowing for the possibility of initial voids with elliptic dynamics evolving free from shell crossings for $t \geq t_i$. This type of graphical illustration is not necessary for parabolic and hyperbolic dynamics, since the no-shell-crossing conditions in these cases (equations (82) and (90), see also Table 1) only depend on the signs of ρ_i, ${}^{(3)}\mathcal{R}_i$ and the contrast functions and can be verified simply by plotting these functions (as in figures 3, 4 and 5). However, for elliptic dynamics the verification of regularity conditions like (100) and (104) is not trivial. In figures (a) and (b) we have density and 3-curvature lumps characterized by the expressions of section VIII. The corresponding parameters are: $[a_1 = b_1 = 1,\ a_2 = 15,\ b_2 = 20,\ f = \sin r]$ and two SC's in figure (a) and $[a_1 = 1,\ b_1 = 0,\ a_2 = 15,\ b_2 = 20,\ f = \tan r]$ and one SC in figure (b). The curves marked by "A" and "B" respectively represent the terms $2\pi P_i[\Delta_i^{(m)} - (3/2)\Delta_i^{(k)}]$ and $P_iQ_i[\Delta_i^{(m)} - (3/2)\Delta_i^{(k)}] - [\Delta_i^{(m)} - \Delta_i^{(k)}]$ appearing in (100). For this regularity condition to hold we need to verify that, for all r, the curve "A" must be larger than that marked by "B" and both curves have to be larger than zero. As shown in (a) and (b) this is what happens for the selected initial value functions (these initial conditions are then used in the elliptic models depicted in figures 10c, 10d, 10e and 10f). In figure (c), the curves marked by "A", "B" and "C" respectively denote the terms $1/2 + (3/2)\Delta_i^{(k)}$, $\Delta_i^{(m)}$ and $\Delta_i^{(k)}$ appearing in (104), calculated for initial value functions characterized by $f = \sin r$, $a_1 = 1.3$, $a_2 = 1$ (density void) and $b_1 = 1$, $b_2 = 1.4$ (3-curvature lump). For (104) to hold, we need (for all r) the curve "C" to be larger than "B" and "B" to be larger than "C", as it happens in the figure. These intial value functions are used in the elliptic model depicted in figure 11b. In general, one might choose the parameters a_1, a_2, f characterizing ρ_i, $\langle\rho_i\rangle$ and $\Delta_i^{(m)}$ from section VIII, then we can always find, by trial and error, the appropriate parameters b_1 and b_2 that comply with (100) and (104).

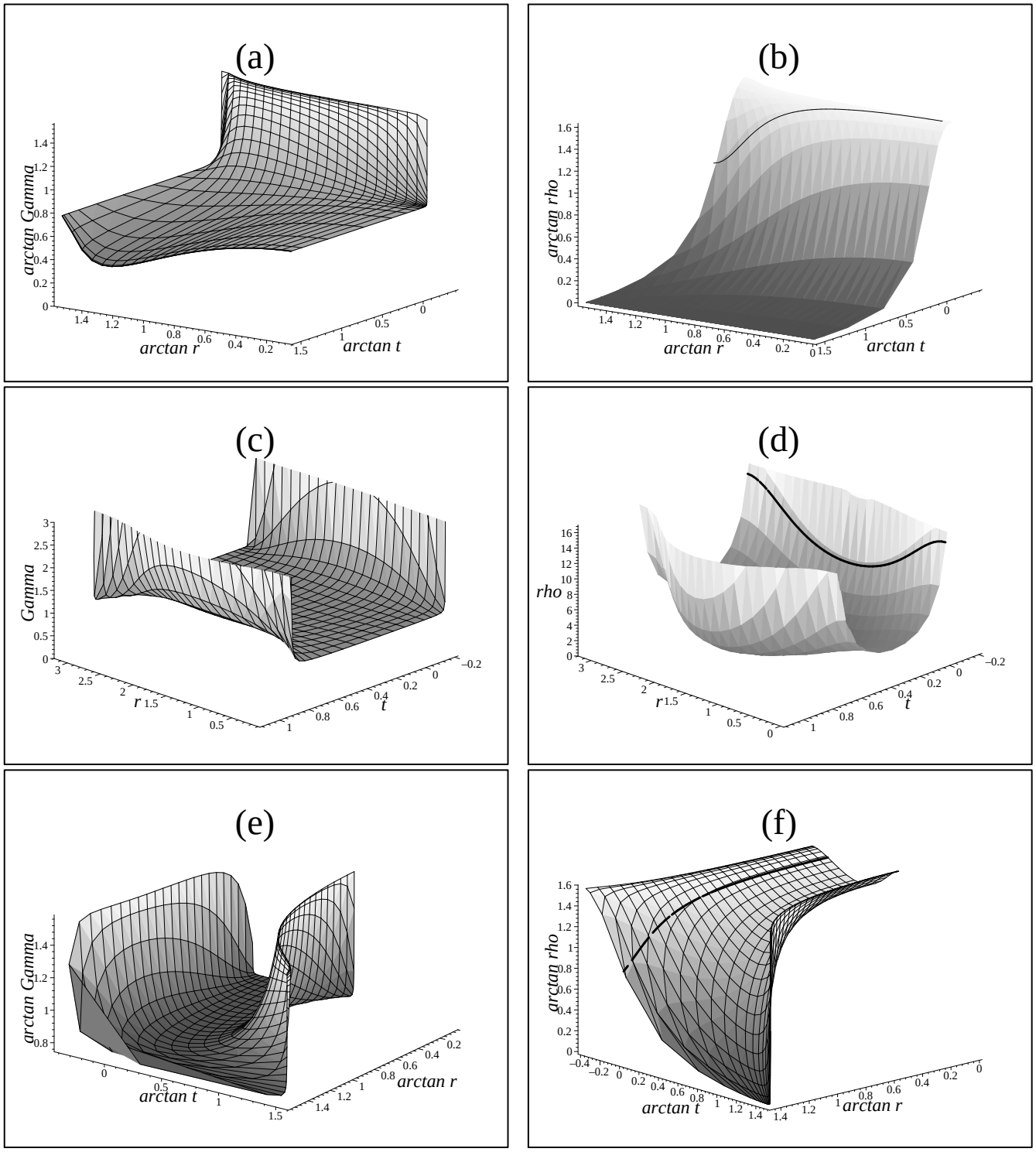

FIG. 10. LTB models free from shell crossings. The function Γ (figures (a), (c) and (e)) and the rest mass density ρ (figures (b), (d) and (f)) are depicted as functions of (t, r) by parametric 3-d plots like in (130). The initial value functions have been selected so that shell-crossings are absent for all the evolution of the models (see Table 1). Figures (a) and (b) correspond to the hyperbolic model characterized by $a_1 = b_1 = 1$, $a_2 = 15$, $b_2 = 20$, $f = \tan r$ (initial density and 3-curvature lumps). Notice in (b) the initial density profile (thick curve in the plotted surface) associated with the initial hypersurface $t = t_i = 0$. Regular models with parabolic dynamics have the same qualitative features as hyperbolic models. The intial value functions associated with the elliptic models in (c), (d), (e) and (f) are those tested in figures 9a and 9b. The models in (c) and (d) have two SC's (hence $f = \sin r$), while those of (e) and (f) have one SC ($f = \tan r$ as those in figures 2e and 2f). Notice in (d) and (f) the initial density profile ρ_i as the thick curve marked by restrcting the 3-d plot to the initial hypersurface $t = t_i = 0$.

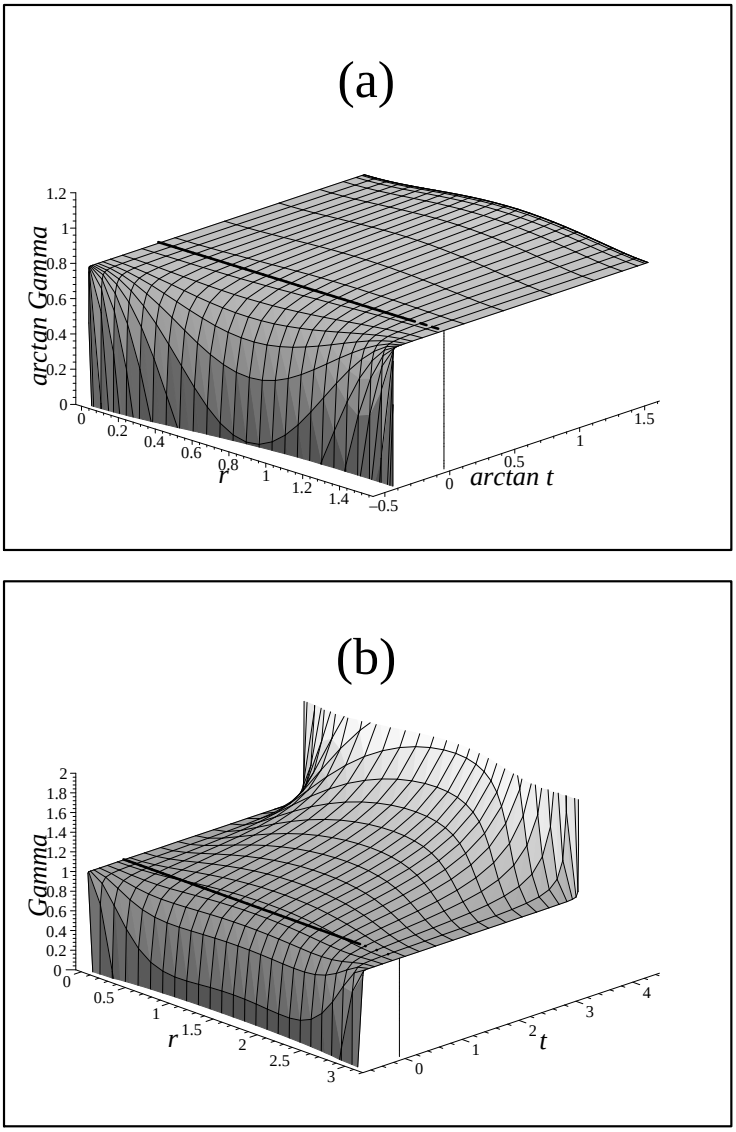

FIG. 11. Models with initial voids that are regular for $t \geq t_i$. These figures depict the parametric 3-d plot of $\Gamma(t, r)$ for models with initial density and 3-curvature voids having hyperbolic (a) and elliptic (b) dynamics. The model in (a) is characterized by $a_1 = b_1 = 1$, $a_2 = 0.45$, $b_2 = 0.5$. Notice that Γ is negative for earlier times but $\Gamma = 1$ along the initial hypersurface $t = t_i = 0$ and $\Gamma > 0$ for all $t \geq t_i = 0$. As long as initial value functions are finite, this type of evolution is possible for all models with parabolic and hyperbolic dynamics and initial value functions characterized as voids. The elliptic model in (b) corresponds to the initial value functions tested in figure 9c. As with the hyperbolic model in (a), the locuus of the shell crossing singularity, $\Gamma = 0$, is confined to times earlier than the initial hypersurface $t = t_i = 0$ (marked as a thick line in the 3-d surface), likewise we have $\Gamma > 0$ for all $t \geq t_i = 0$. As shown in figures 7d and 7e, the locuus of $\Gamma = 0$ in elliptic models with initial voids will exhibit, in general, two branches (as the locuus of $y = 0$). Condition (104), leading to a single branched form for $\Gamma = 0$, is a strong restriction on the initial conditions of elliptic models. We used in (b) the elliptic model with two SC's but a very similar plot emerges by considering the case with one SC.

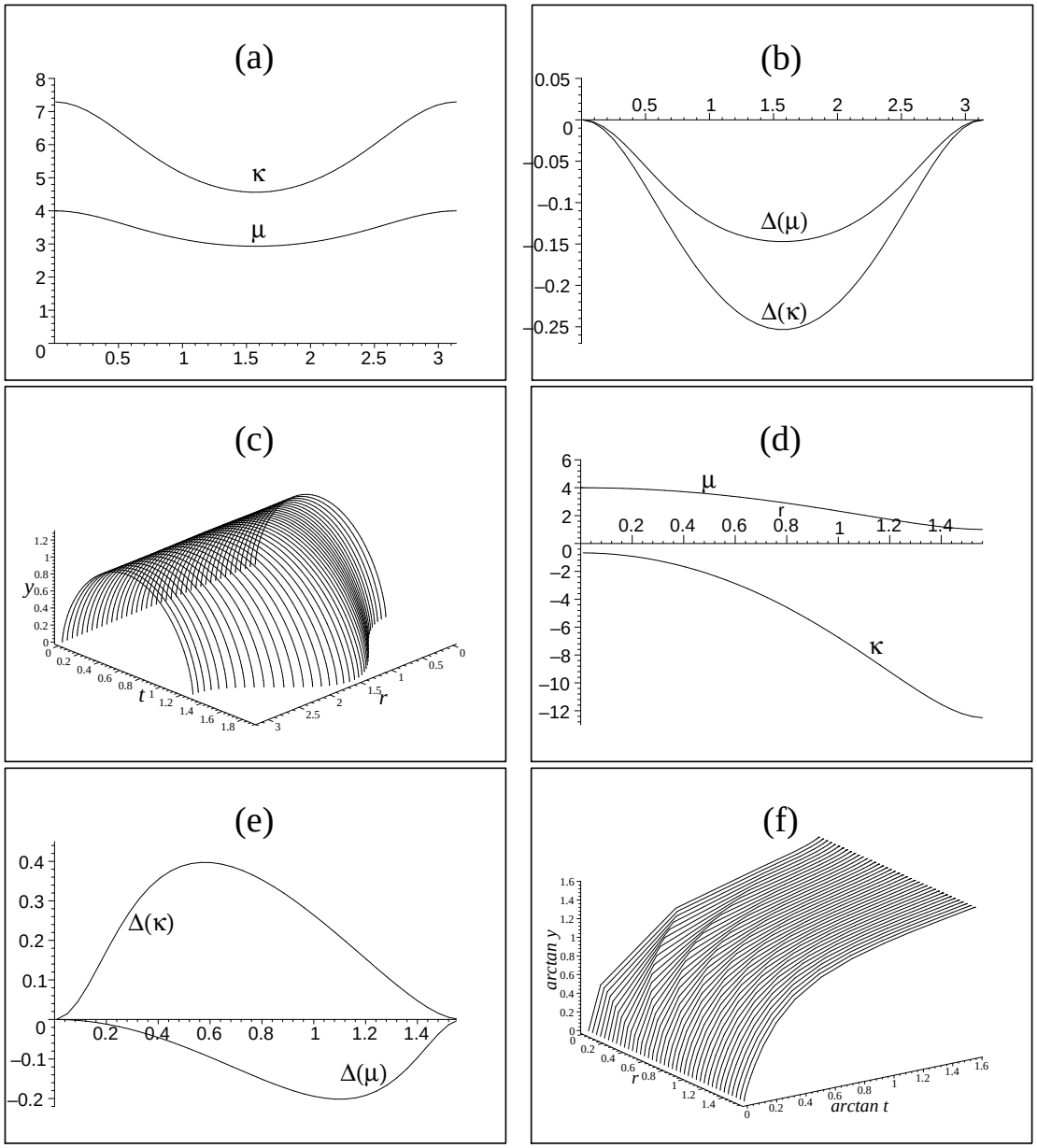

FIG. 12. Models with a simmultaneous big bang. We consider models with elliptic (figures (a), (b) and (c)) and hyperbolic (figures (d), (e) and (f)) dynamics. We select μ and $\Delta_i^{(m)}$ from equations (122) and (124) and find κ and $\Delta_i^{(k)}$ by solving numericaly equations (108), (109) for the hyperbolic case and (111), (112) for the elliptic case. The functions μ and $\Delta_i^{(m)}$ are characterized by $a_1 = 1$, $a_2 = 4$ and $f = \sin r$, $\tan r$, respectively, for the elliptic and hyperbolic case (we can assume that $4\pi G\bar{\rho}_i/c^4 = 1$). For the numerical solutions we have taken the constant bang time in (109) and (112) to be $t_{bb}^{(0)} = 0.23$ (hyperbolic) and $t_{bb}^{(0)} = 0.4$ (elliptic), for an initial hypersurface marked by $t = t_i = 1$. The values of $t_{bb}^{(0)}$ are not arbitrary and depend on the choice of t_i, μ and $\Delta_i^{(m)}$. Figures (a) and (b) display the obtained κ and $\Delta_i^{(k)}$ plotted next to the selected μ and $\Delta_i^{(m)}$ (both contrast functions have the same sign, as required by (110)). Figure (c) displays the parametric 3-d plot $y(t, r)$ that corresponds to the full set of intial value functions. Notice that a simmultaneous big bang does not imply (in general) a simmultaneous "big crunch". Figures (d) and (e) display the corresponding initial value functions for the hyperbolic model (notice that the contrast functions have opposite signs, as required by (107)). The parametric 3-d plot $y(t, r)$ for the hyperbolic case is shown in (e).

APPENDIX: INVARIANTS AND GENERIC FEATURES OF LTB SOLUTIONS.

- Kinematic invariants. For (1) and (2), we have $\dot{u}_a = u_{a;b}\,u^b = 0$, so that the 4-velocity is a geodesic field, while the expansion scalar and shear tensor are

$$u^a{}_{;a} \equiv \Theta = \frac{\dot{Y}'}{Y'} + \frac{2\dot{Y}}{Y}, \tag{A1}$$

$$\sigma^a{}_b = \mathbf{diag}\,[0, -2\sigma, \sigma, \sigma]\,, \qquad \sigma \equiv \frac{1}{3}\left(\frac{\dot{Y}}{Y} - \frac{\dot{Y}'}{Y'}\right), \qquad \sigma_{ab}\,\sigma^{ab} = 6\sigma^2, \qquad \frac{\Theta}{3} + \sigma = \frac{\dot{Y}}{Y}, \tag{A2}$$

- Curvature scalars.. The Ricci scalar, ${}^{(3)}\mathcal{R}$, of the 3-dimensional hypersurfaces of constant t (rest frames of comoving observers) can be expressed in terms of ρ, Θ and σ by the equation

$$\frac{c^2}{6}\,{}^{(3)}\mathcal{R} \;=\; \frac{8\pi G}{3c^2}\,\rho \;-\frac{1}{9}\,\Theta^2 \;+\; \sigma^2 \;=\; -\frac{c^2\,(E\,Y)'}{3\,Y^2 Y'}, \tag{A3}$$

The 4-dimensional Ricci scalar, Ricci tensor squared and Riemann tensor squared (the Kretschmann scalar) are

$$\mathcal{R} \;=\; \frac{8\pi G}{c^4}\,\rho, \qquad \mathcal{R}_{ab}\,\mathcal{R}^{ab} \;=\; \mathcal{R}^2$$

$$\mathcal{R}_{abcd}\,\mathcal{R}^{abcd} \;=\; \frac{4}{3}\left(\frac{6\,M}{Y^3} \;-\; \mathcal{R}\right)^2 \;-\; \frac{5}{3}\,\mathcal{R}_{ab}\,\mathcal{R}^{ab} \;=\; \left(\frac{8\pi G}{c^4}\right)^2\left[\frac{4}{3}\left(\frac{3\,m}{Y^3} \;-\; \rho\right)^2 \;+\; \frac{5}{3}\,\rho^2\right], \tag{A4}$$

while the electric part of the conformal Weyl tensor, $E^a{}_b \equiv C_{abcd}u^a u^b$, is given in terms of the only nonzero invariant Weyl curvature scalar, ψ_2, by

$$E^a{}_b \;=\; \mathbf{diag}\,[0, -2\psi_2, \psi_2, \psi_2], \qquad \psi_2 \;=\; \frac{4\pi G}{3c^4}\left[\;\frac{3\,m}{Y^3} \;-\; \rho\;\right] \;=\; \frac{M}{Y^3} \;-\; \frac{4\pi G}{3c^4}\,\rho, \tag{A5}$$

- Regularity and differentiability..

Spherical symmetry is characterized by the group SO(3) acting transitively along 2-spheres (orbits) with proper area $4\pi\,Y^2(t,r)$. The domain of regularity of LTB solutions can be given then as the set of all spacetime points marked by (t,r) for which (a) $Y \geq 0$ and (b) all curvature scalars (like those in (A3), (A4) and (A5)) are bounded.

Minimal differentiability requirements for the basic variables can be summarized as follows [16], [18]: Y and all its time derivatives are continuous, while quantities involving radial derivatives like Y', $\dot{Y}'$, Y'', etc can be piecewise continuous, thus allowing jump discontinuities for a countable number of values $r = r_1$ so that the right and left limits as $r \to r_1$ are different but this difference is always finite. These conditions imply (via (3)) that the basic variables Y, M, E, $t_{_{bb}}$ must be at least continuous (ie C^0), while ρ and other quantities (Θ, σ, ${}^{(3)}\mathcal{R}$, ψ_2) containing terms like Y' or $\dot{Y}'$ could be piecewise continuous.

From (4), the weak energy condition leads to

$$\rho \;\geq\; 0 \qquad \Leftrightarrow \qquad \mathrm{sign}(Y') \;=\; \mathrm{sign}(M'), \tag{A6}$$

while regularity of the metric component g_{rr} requires

$$1 \;+\; E \;\geq\; 0, \tag{A7}$$

a condition that is trivialy satisfied for parabolic and hyperbolic ($E \geq 0$), but not for elliptic solutions or regions ($E < 0$). The equality in (A7) implies that Y' and E must have a common zero of the same order (see below).

- Zeroes of Y and Y'

  The functions Y and Y' can vanish, either for a value $r = \text{const.}$, or for a coordinate locuus (t, r) with $r \neq \text{const}$. The two cases lead to very different situations:

  - Zeroes of Y for $r = r_c$ (Symmetry centers, SC).
    These regular worldlines marked by $r = r_c$ are the worldlines of fixed points of SO(3). LTB solutions (like all sphericaly symmetric spacetimes) admit zero, one or two SC's. They are characterized by $Y(t, r_c) = \dot{Y}(t, r_c) = 0$. All of $M(r_c)$, $M'(r_c)$, $E(r_c)$, $E'(r_c), t'_{bb}(r_c)$ vanish at a SC, but the order of the zeroes of these functions (power of leading terms) follows from the regularity of each term in (3). Near $r = r_c$ we have [16], [17], [18]

    $$Y \approx Y'(t, r_c)(r - r_c), \qquad M \approx M'''(r_c)(r - r_c)^3, \qquad E \approx E''(r_c)(r - r_c)^2, \qquad t_{bb} \approx t''_{bb}(r_c)(r - r_c)^2, \quad \text{(A8)}$$

  - Zeroes of Y for non-comoving locii (Central singularities).
    All curvature scalars, such as (A3), (A4) and (A5), diverge as the proper area of the orbits of SO(3) vanish, hence the name "central" (associated with singular centers). By analogy with FLRW spacetimes and depending on whether dust layers expand or collapse, these singularities are called a "big bang" or a "big crunch". These singularities cannot be avoided for any choice of free parameters, thus they are an essential feature of LTB models.
  - Zero of Y' for $r = r^*$ (Turning values of Y' and surface layers).
    The extrinsic curvature forms of the 3-dimensional submanifolds $r = \text{const.}$ must be continuous (at least C^0) as r increases. If if $Y'(t, r^*) = 0$ for a comoving $r^* \neq r_c$, these extrinsic curvature forms are continuous as $r \to r^*$ as long as the following regularity conditions hold [4], [16], [17], [18]

    $$Y'(t, r^*) \;=\; 0 \qquad \Leftrightarrow \qquad M'(r^*) \;=\; 0, \qquad 1 \;+\; E(r^*) \;=\; 0, \quad \text{(A9)}$$

    implying that the common zero, $r = r^*$, of Y', M', $1 + E$ is of the same order in $r - r^*$. If these conditions fail to hold, the extrinsic curvature of hypersurfaces $r = \text{const.}$ is discontinuous as $r \to r^*$ and we have a surface layer at $r = r^*$ (see [30], [4], [16], [17], [18]).
  - Zeroes of Y' for non-comoving locii (Shell crossing singularities).
    From (4), energy density ρ diverges (and thus all curvature scalars like (A3), (A4) and (A5) diverge). Since g_{rr} vanishes for (in general) $Y > 0$, proper distances between comoving layers vanish, hence the name "shell crossing". Unlike central singularities, shell crossings are unphysical and are not esential. Conditions for having LTB models free from these singularities can be given in terms of M, E, t_{bb} and their gradients (see section VII, Table 1 and references [15], [16], [17], [18]).

- "Open" or "closed" models. Hypersurfaces $t = \text{const}$, $\mathcal{T}$, are everywhere orthogonal to the 4-velocity vector field u^a, hence they can be characterized invariantly as the rest frames of comoving observers associated with the metric

  $$h_{ab} \;=\; u_a\, u_b \;+\; g_{ab} \quad \text{(A10)}$$

  All $\mathcal{T}$ are Cauchy hypersurfaces [7] in LTB solutions. They are foliated by 2-spheres marked by constant values of r. However, the radial coordinate can be arbitrarily rescaled, and so an invariant measure of distances along its direction is given by the proper length integral $\ell = \int \sqrt{g_{rr}} dr$, evaluated for spacelike curves with fixed (θ, ϕ). For a regular and maximaly extended hypersurface, the domain of r is limited, either by SC's (since $Y \geq 0$) and/or by maximal values $r = r_{\max}$ defined by

  $$\ell \;=\; \int \frac{Y' dr}{\sqrt{1 \,+\, E}} \;\to\; \infty \qquad \text{as} \qquad r \;\to\; r_{\max}, \quad \text{(A11)}$$

  The terms "open" and "closed" respectively corresponds to an infinite or finite proper volume of these hypersurfaces, evaluated from (1) as

  $$V \;=\; 4\pi \int \frac{Y^2 Y' dr}{\sqrt{1 \,+\, E}}, \quad \text{(A12)}$$

where the integral must be evaluated along all the domain of r. The class of homeomorphism of hypersurfaces $t =$ const. is related the number of SC's (see section VI-C for more details). From familiarity with FLRW spacetimes, one would tend to expect a "natural" association between closed topologies with elliptic (recollapsing) dynamics and open topologies with parabolic or hyperbolic dynamics. However, this association need not be mandatory (see [15], [12] and sections VI and VIII): open topologies might have elliptic dynamics and closed topologies might present parabolic or hyperbolic evolution, though in this last case a surface layer appears at $r = r^*$ such that $Y'(t, r^*) = 0$ (see [30], [4], [16] and [18]).